ATCH 6

REPORT DOCUMENTATION PAGE

Form Approved
OMB No. 0704-0188

Public reporting burden for this collection of information is estimated to average 1 hour per response, including the time for reviewing instructions, searching existing data sources, gathering and maintaining the data needed, and completing and reviewing the collection of information. Send comments regarding this burden estimate or any other aspect of this collection of information, including suggestions for reducing this burden, to Washington Headquarters Services, Directorate for information Operations and Reports, 1215 Jefferson Davis Highway, Suite 1204, Arlington, VA 22202-4302, and to the Office of Management and Budget, Paperwork Reduction Project (0704-0188), Washington, DC 20503.

1. AGENCY USE ONLY (Leave blank)	2. REPORT DATE	3. REPORT TYPE AND DATES COVERED
	04/28/96	Final Tech. Rpt. 3/01/93 - 2/29/96

4. TITLE AND SUBTITLE
Investigation of Active Control of Combustion Instabilities in Chemical Rockets

5. FUNDING NUMBERS
F-49620-93-1-0177

6. AUTHOR(S)
Ben T. Zinn
Brady R. Daniel
Yedidia Neumeier

7. PERFORMING ORGANIZATION NAME(S) AND ADDRESS(ES)
Georgia Institute of Technology
School of Aerospace Engineering
Atlanta, Georgia 30332-0150

8. PERFORMING ORGANIZATION REPORT NUMBER

9. SPONSORING / MONITORING AGENCY NAME(S) AND ADDRESS(ES)
AFOSR/NA
110 Duncan Avenue, Sutie B115
Bolling AFB, DC 20332-0001

NA

AFOSR-TR-96
0273

11. SUPPLEMENTARY NOTES

12a. DISTRIBUTION / AVAILABILITY STATEMENT
Approved for public release; distribution is unlimited

12b. DISTRIBUTION CODE

13. ABSTRACT *(Maximum 200 words)*

This report summarizes the main accomplishments of a three-year research program supported under AFOSR Grant No. F49620-93-1-0177. The main objective of this program was to investigate active suppression of detrimental combustion instabilities in chemical rockets by a controlled, secondary, combustion process. The program consisted of parallel theoretical and experimental efforts; the former developed the theoretical foundation of the investigated control approach and the latter developed a small scale, actively controlled, gas rocket setup that was used to guide the development of the investigated active control system and demonstrate its effectiveness.

19960614 088

14. SUBJECT TERMS	15. NUMBER OF PAGES
	65
	16. PRICE CODE

17. SECURITY CLASSIFICATION OF REPORT	18. SECURITY CLASSIFICATION OF THIS PAGE	19. SECURITY CLASSIFICATION OF ABSTRACT	20. LIMITATION OF ABSTRACT
unclassified	unclassified	unclassified	unlimited

DTIC QUALITY INSPECTED 1

AFOSR FINAL REPORT

on

INVESTIGATION OF ACTIVE CONTROL OF COMBUSTION INSTABILITIES IN CHEMICAL ROCKETS

Prepared for

Air Force Office of Scientific Research
Aerospace Sciences Directorate
Bolling Air Force Base

by

Ben T. Zinn
Brady R. Daniel
Yedidia Neumeier

School of Aerospace Engineering
Georgia Institute of Technology
Atlanta, GA 3032

March 1996

Approved for public release; distribution unlimited
AFOSR Grant No. F49620-93-1-0177

Summary

This report summarizes the main accomplishments of a three-year research program supported under AFOSR Grant No. F49620-93-1-0177. The main objective of this program was to investigate active suppression of detrimental combustion instabilities in chemical rockets by a controlled, secondary, combustion process. The program consisted of parallel theoretical and experimental efforts; the former developed the theoretical foundation of the investigated control approach and the latter developed a small scale, actively controlled, gas rocket setup that was used to guide the development of the investigated active control system and demonstrate its effectiveness.

The developed active control system (ACS) consists of a pressure transducer that continuously measures the combustor's pressure, an observer that analyzes the measured pressure and determines the amplitudes, phases and frequencies of the unstable combustor modes in real time, a controller that provides each identified mode (by the observer) with a phase shift and a gain and generates a control signal that is sent to a fuel injector actuator that modulates the injection rate of a secondary fuel stream into the combustor. This control system is based upon Rayleigh's criterion and designed to produce a secondary, oscillatory, combustion process within the combustor that is out of phase with the combustor pressure oscillations, thus resulting in their attenuation.

The theoretical efforts investigated the performance of an actively controlled rocket motor that is prone to axial instabilities. Two models that investigated the control of axial instabilities were developed. The first used an approximate, Galerkin type, approach to study the control of linear instabilities and the second used a heuristic model and a numerical solution approach to investigate the performance of an actively controlled rocket. The latter used a phenomenological model to describe combustor mixing processes and global, Arrhenius type, global kinetics to describe the combustion processes. These models were used to predict the conditions within the combustor with the ACS on and off. The control of both linear and nonlinear instabilities was investigated. These studies demonstrated that the developed ACS can identify the characteristics of severe instability in practically real time and effectively damp each unstable mode. Furthermore, numerical predictions of the combustor response to open loop control were found to be in good agreement with experimental results. Finally, these studies developed improved means for the numerical representation of the injector face boundary condition and the handling of various sources (e.g., heat and mass addition, area change and friction) in Roe's Rieman scheme, which was used to numerically solve the model equations.

The experimental efforts developed an actively controlled gas rocket that was subsequently used to investigate the performance of the ACS in open and closed loop control modes. The open loop studies developed two approaches for determining the frequency dependence of the fuel injector actuator-combustor system response. The results of these studies were stored in the ACS' controller and used to determine the phase shift and gain that controller must add to the unstable combustor modes in closed loop control. Subsequent, closed loop, control studies showed that the investigated ACS can effectively damp large amplitude, highly nonlinear, instabilities in periods of the order of 40 milliseconds, which are considerably shorter than the times reported by other investigators.

The main contributions of this study are:

1. the development of an active control approach based upon Rayleigh's criterion,

2. the development and demonstration of an observer that determines the amplitudes, phases and frequencies of a prespecified number of unstable, combustor modes in real time,

3. the development of theoretical models for investigating active control of linear and nonlinear instabilities in rocket motors,

4. the development of a fuel injector actuator that utilizes a magnetostrictive material to modulate a secondary fuel injection rate over a 0-1,200 Hz. range, which is wider than that of any known injector,

5. the demonstration that the developed fuel injector actuator can excite significant reaction rate heat release oscillations within the combustor,

6. the development of two different approaches for determining the frequency dependence of the response of the secondary combustion process generated by the fuel injector actuator, and

7. the demonstration that closed loop application of the investigated ACS significantly (e.g., by 26 dB.) and rapidly (e.g., within 40 milliseconds) damps a rocket motor instability without destabilizing any stable modes.

It is believed that these findings provide a foundation for guiding the development of ACS for unstable rockets and other combustors. The results of this program have been demonstrated to a number of companies. A major gas turbine manufacturer is currently working on adapting the developed ACS technology for application in unstable gas turbines, and a fuel injector actuator based upon the one developed under this program is being investigated by the Navy for application in active control of shipboard incinerators.

Introduction

This report describes the results of a three-year investigation of active control of combustion instabilities in chemical rockets. Such instabilities are generally driven by a feedback-type interaction between flow and combustion process oscillations; energy supplied by an oscillatory combustion process produces oscillatory heat release that excites one or more natural acoustic modes of the combustor whose oscillations are responsible for the periodicity of the combustion process. The condition for driving an instability in a combustor can be expressed by the following modified form of Rayleigh's criterion:

$$\int_V \int_T p'(x,t)Q'(x,t)dtdV \geq \int_V \int_T \sum_i L_i(x,t)dtdV \qquad (1)$$

where p', Q', L_i, t, x, T and V are the combustor pressure oscillation, heat addition oscillation, i-th loss process (e.g., viscous dissipation, acoustic energy transmission through the nozzle), time, location within the combustor, period of the oscillation and combustor volume, respectively. The integral on the left and right hand side of Eq. 1 describes the total driving and damping experienced by the combustor oscillations, respectively. An instability occurs when the inequality in Eq. 1 is satisfied; that is, the overall driving within the combustor is larger than the overall combustor damping. It is noteworthy that driving occurs at a given location x when the time integral on the left side of Eq. 1 is positive at that location. This condition is satisfied when magnitude of the phase difference ϕ between the pressure and heat addition oscillations is less than 90 degrees. It follows that at locations where the magnitude of this phase difference is larger than 90 degrees, the oscillatory heat addition process damps the oscillations.

An examination of Eq. 1 suggests that instabilities could be prevented by decreasing the magnitude of the integral on the left and/or increasing the magnitudes of various loss terms on the right. The former can be attained by modifying the characteristics of the combustion process and/or its interaction with the flow oscillations. The characteristics of the combustion process could be changed by, for example, modifying the propellants' feed system, fuel injectors and propellants' composition. On the other hand, the loss terms on the right hand side of the Eq. 1 could be increased by, for example, changing the characteristics of the nozzle and/or adding mechanical elements (e.g., an acoustic liner) that dissipate acoustic energy in the combustor. These control approaches are generally referred to as passive, and their effective implementation requires understanding of the mechanisms that drive the instability, the characteristics of the excited oscillations, and the losses produced by various system elements.

Unfortunately, passive control approaches have generally not been satisfactory. Lack of adequate understanding of the fundamental processes that control the instability resulted in "solutions" there were only applicable to a specific combustor design over a limited range of operating conditions. Consequently, different passive control approaches had to be developed for different unstable combustors. Since these passive control approaches were generally developed in costly and lengthy trial-and-error development programs, it became apparent that new approaches for controlling combustion instabilities are needed.

The considerable progress in the areas of computers, electronics, sensors, actuators and control theory in recent years has renewed interest in the development of active control systems (ACS) for preventing combustion instabilities. An ACS can prevent the onset and/or damp an instability by one or more of the following actions:

1. production of heat addition oscillations in the combustor that are 180 degrees out of phase relative to the unstable pressure oscillations, thus resulting in their attenuation (based upon Rayleigh's criterion; see Eq. 1 above), and/or

2. interference with the mechanisms that drive the instability in a way that reduces their driving effectiveness, and/or

3. modification of the system's boundary condition(s) in a way that produces one or all the following: (i) increase in the system's damping, (ii) modification of the modes that can be excited within the system, and (iii) destructive interference with the mechanisms that drive the instability.

A typical ACS generally consists of a sensor, an observer, a controller, and an actuator, see Fig. 1. The sensor (e.g., a pressure transducer or a photo-multiplier) continuously "senses" the conditions inside the unstable combustor. The signal measured by the sensor is transmitted to the observer that determines the state of the system. This information is sent to the controller where it is modified, using a specific control approach, and sent to the actuator that "perturbs" the combustor in a controlled manner. The latter prevents the onset or damps the instability via one or more of the actions described in Items 1-3 above.

The main advantages of a given ACS are:

1. it can prevent the onset and/or rapidly attenuate combustion instabilities,

2. it can rapidly respond to changes in the combustor operating conditions and, thus, the characteristics of the instability, and

3. it is expected to be applicable (perhaps with some modifications) to different unstable combustors, thus providing a capability for effective control of instabilities in a variety of combustion systems.

While prior investigations of active control of combustion instability had demonstrated the considerable promise of this approach, a close examination of the results of these studies revealed that much remained to be done in several areas before active control can be implemented in practical combustors. For example, past investigations generally filtered the measured signal before sending it to the controller where it was amplified and phase shifted before being sent to the actuator. The use of a filter requires, however, apriori knowledge of the frequency of the instability. While this frequency can be readily determined in advance in experimental combustors, it is generally not known apriori in practical combustors, and may vary in response to changes in combustor operating conditions. Consequently, a practical ACS should possess capabilities for determining in real time the frequencies of the unstable combustor modes. Another problem is the shortcomings of actuators such as loudspeakers, mechanical valves and fuel injectors that had been utilized by other investigators. For example, loudspeakers generally don't have the power required for stabilizing practical combustors, capabilities for continuous operation without failure, and "hardware" that can survive in hostile combustor environments. Similarly, mechanical valves are complex, heavy and limited to low frequency applications. It, thus, became apparent at the outset of this program that a fuel injector that can supply an oscillatory fuel flow rate into the combustor to drive pressure oscillations at a desired frequency and phase and/or modify the primary combustion process in a manner that reduces its driving effectiveness should be used as the actuator in an ACS for damping combustion instabilities. The automotive fuel injectors that were utilized in past studies are limited, however, to low frequencies and low fuel flow rates and, consequently, are not suitable for use in practical ACS.

In an effort to advance the state of the art and develop capabilities that would lead to the development of practical active control systems for unstable rocket (and other) combustors, efforts under this program focused on developing the following capabilities:

1. an observer that can analyze the sensor's signal and determine in the amplitudes, frequencies and phases of up to five unstable combustor modes in virtually real time,

2. a fuel injector actuator that can modulate the flow rate of a gaseous fuel with significant amplitudes over a 0-1,200 Hz. frequency range, whose upper limit is considerably higher than the maximum frequency of any known (e.g., automotive) fuel injector,

3. a small scale, actively controlled, variable length, gas rocket that exhibits axial instabilities, similar to those observed in full scale rocket motors, over a wide range of frequencies (e.g., 100-1800 Hz.), and

4. a model of an actively controlled gas rocket that can be used to theoretically investigate the performance of various ACS and control strategies.

The research activities and accomplishments of this program are described in the remainder of this report. These are described in the following order: 1. the principles of operation of the investigated ACS, 2. theoretical investigations of the performance of unstable rocket motors actively controlled with the investigated ACS, 3. the developed experimental setup, 4. open loop active control performance of the investigated ACS, 5. closed loop active control of combustion instabilities with the investigated ACS, and 6. summary and conclusions of the results of this program.

The Investigated Active Control System

At the onset of this program it was recognized that an ACS capable of preventing detrimental rocket motor instabilities will require capabilities for:

1. identification of the characteristics of all the unstable combustor modes in virtually real time (i.e., before the instability results in rocket malfunction) using limited sensor data about the combustor performance,

2. determination of the appropriate phase and gain that must be "added" by the controller to each unstable mode and generation of an appropriate control signal for the actuator, and

3. means for introducing controlled "perturbations" into the combustor that will attenuate the unstable combustor modes.

To provide these capabilities, the developed ACS uses a pressure transducer installed near the combustor's injector as its sensor, because the anti-nodes of most potentially unstable axial pressure oscillations are likely to occur near this location. This maximizes the likelihood that the measured pressure will include contributions from all unstable combustor modes. The measured pressure is then transmitted to an observer whose task is to determine, in virtually real time, the amplitudes, frequencies and phases of all combustor modes that significantly contribute to the instability. The identified characteristics of the unstable modes are transmitted to a controller where each mode is provided with a gain and a phase shift that will result in the attenuation of the corresponding mode within the combustor. The controller combines the modified modes into a single signal that is sent to a fuel injector actuator that can modulate the injection rate of a gaseous fuel into the combustor over a 0-1,200 Hz. frequency range. The fuel injection modulations produce reaction rate and heat addition oscillations within the combustor at the frequency of the fuel flow rate modulation. These heat addition oscillations should, according to Rayleigh's criterion, damp the instability if the magnitude of the phase difference between these heat addition and combustor pressure oscillations is smaller than ninety degrees.

The Observer

Since the developed observer plays a key role in the investigated ACS and it is repeatedly referred to in the remainder of this report, its principles of operation are presented in this section.

The observer analyzes the measured pressure to determine in real time the amplitudes, phases, and frequencies of the unstable combustor modes. It assumes that the measured combustor

pressure p(t) can be expressed as the following sum of combustor modes that may not be harmonics of one another and may have frequencies, amplitudes and phases that slowly vary with time.

$$p(t) = \sum_{n=1}^{n=k} S_n \sin(\omega_n t) + C_n \cos(\omega_n t) \qquad (2)$$

The observer determines the characteristics of the dominant (i.e., largest amplitude) mode by solving the integrals

$$S_n(t) = \frac{2}{T_n} \int_{t-T_n}^{t} \sin(\omega_n t) p(t) dt; \; C_n(t) = \frac{2}{T_n} \int_{t-T_n}^{t} \cos(\omega_n t) p(t) dt \qquad (3)$$

where the oscillation period T_n and frequency ω_n are related by $T_n = 2\pi / \omega_n$ and are not known apriori. It can be shown that the above integrals can replaced by following recursive formulae:

$$S_n(t + \Delta t) = S_n(t) + \frac{2}{T_n}\left(p(t + \Delta t) - p(t - T_n + \Delta t)\right) \cdot \sin(\omega_n t) \cdot \Delta t \qquad (4\text{-a})$$

$$C_n(t + \Delta t) = C_n(t) + \frac{2}{T_n}\left(p(t + \Delta t) - p(t - T_n + \Delta t)\right) \cdot \cos(\omega_n t) \cdot \Delta t \qquad (4\text{-b})$$

whose solution requires little computational effort[1]

The unknowns $S_n(t)$, $C_n(t)$ and ω_n are determined in a rapidly converging iterative solution procedure. Initially, a value for ω_n (and, thus, T_n) is assumed and substituted into Eqs. 4, which are then solved for the "corrected" coefficients of $S_n(t+Dt)$ and $C_n(t+Dt)$. The calculated coefficients are then substituted into the following relationship[1] that determines a corrected value of the frequency:

$$\left[(\omega)^2\right]^{t+\Delta t} = \left[\omega^2 + \frac{\omega\left(\frac{ds}{dt}\sin(\omega t) + \frac{dc}{dt}\cos(\omega t)\right)}{S \bullet \cos(\omega t) - C \bullet \sin(\omega t)} \right]^{t} \qquad (5)$$

where the subscript 'n' has been omitted for simplicity. The values of ω on the left and right sides of Eq. 5 are the "corrected" and "previous calculated" values of the frequency, respectively. Once a corrected value of ω is obtained from Eq. 5, the corresponding period T is substituted into Eqs.

4 to obtain improved values of S(t) and C(t). This procedure rapidly converges into the "final" values of the unknowns ω, S and C, which are then used to determine he amplitude, phase and frequency of the dominant mode. This procedure can also track "slow" variations of these quantities. Once the characteristics of the dominant mode are known, the expression describing its time dependence is subtracted from the measured pressure p(t) and the above procedure is repeated to determine the characteristics of the "next" dominant mode within the remaining signal.

The above described procedure can be repeated to determine the characteristics of as many modes as desired. Clearly, the need to attain real time identification of the characteristics of an instability would limit the number (e.g., two or three) of modes that can be identified. This is not, however, a problem as most instabilities are generally dominated by one or two modes.

Figures 2-a through 2-e demonstrate the ability of the observer to identify in real time the hierarchy of modes in an unstable combustor. The observer was provided with the pressure signal shown in Fig. 2-a, which was measured in the gas rocket motor that was developed under this program when it experienced combustion instability. Figure 2-a shows that the instability "switches" from low to high frequency oscillations between .05 and .064 seconds. This signal was analyzed by the observer and the computed frequencies and amplitudes were used to determine the time dependence of the two most dominant combustor modes, see Figs. 2-b through 2-e. Figures 2-b shows that the frequency of the nearly sinusoidal, dominant, mode abruptly increases around .065 seconds to that of the second mode, while Fig. 2-c shows that the second mode oscillates with a higher frequency and its amplitudes decreases to practically zero around .065 seconds. Figures 2-b,c also show that the observer can simultaneously track the behavior of both modes in real time. Figure 2-d presents the calculated time dependence of the frequencies of the two observed modes. It shows that the observed frequency of the dominant mode changed from 650 to 1250 Hz. within only three milliseconds. Finally, Fig. 2-e compares the measured pressure p(t) with that obtained by synthesis of the two observed modes. It clearly shows that the observer can "reproduce" the input pressure in real time and with high fidelity.

During the last year of this program a theoretical study aimed to extend the initially developed observer approach to provide a capability for simultaneous identification of several unstable modes was undertaken. This study is presented in Appendix A. While the current observer determines the characteristics of the unstable modes in a hierarchical manner (i.e., the most dominant mode is identified first, then the next mode dominant mode is identified and so on), the new approach simultaneously identifies the characteristics of several unstable combustor modes. It is expected that the results of this study will increase the accuracy and robustness of the observer and increase the likelihood that its output will converge to the correct results.

Theoretical Studies

The performance of the investigated ACS, see Fig. 1, was initially theoretically studied by solving the system of one dimensional, unsteady, conservation equations that modeled the flow in an unstable combustor[2]. The model assumed that the instability is driven by a simple linear feedback between the pressure and combustion process heat addition oscillations. The unstable combustor model was then "equipped" with the developed ACS and used to theoretically investigate the effectiveness of the developed ACS. Numerical simulations showed that the developed ACS can rapidly damp a variety of instabilities including, for example, combustor acoustic mode oscillations with amplitudes equaling twenty-five percent of the mean combustor pressure, which were damped within a few milliseconds after activating the ACS.

Subsequent studies developed a heuristic model of an unstable gaseous rocket combustor and an improved numerical approach for solving the model equations. The conservation equations solved by this model are summarized in Fig. 3. Since the model assumes that the combustor flow is one dimensional and inviscid, and, thus, cannot account for turbulent mixing, a phenomenological mixing model that describes the mixing of the premixed reactants with the hot combustion products has been incorporated into the conservation equations (i.e., see terms proportional to $1/\tau_{mix}$). This model also accounts for the mixing of the secondary fuel, injected by the fuel injector actuator, with the combustor flow before its reaction. The magnitude of the spatial dependence of the mixing process is controlled by the function W(x), see Fig. 3, which depends upon a prespecified mixing length l_{mix}. Once a combustible mixture is formed, the combustion process heat release rate is controlled by global, Arrhenius type, methane kinetics, which is the fuel used in the experimental phase of the program.

Once it had been shown that the heuristic model predicts unstable rocket operation of ranges of design and operating parameters, the model was "equipped" with the investigated ACS and the resulting model was used to investigate the behavior of an actively controlled rocket motor. Typical results obtained in this study are presented in Figs. 4 and 5. Figure 4 shows predictions of the motor's performance under open loop control excitation. It shows predicted time dependence of pressure and heat release oscillations within the rocket combustor when the fuel injector actuator modulated the secondary fuel injection rate at specific frequency. The results show that the actuator can excite significant pressure and heat release oscillations within the combustor, indicating that it could serve as an actuator in closed loop control of rocket motor combustion instabilities. An analysis of the time dependence of the results shows that the heat release oscillations lead the pressure oscillations and that the magnitude of the phase difference is always

smaller than ninety degrees, in agreement with Rayleigh's criterion. This phase difference decreases as the amplitude of the excited oscillations increases, and it approaches ninety degrees as the growth grate of the oscillations decreases, indicating that less driving is needed when the amplitude growth rate goes to zero.

Figure 5 presents predictions of the effect of closed loop control upon the oscillations in an unstable rocket combustor. The two top plots show the onset, growth and decay of the instability before and after the activation of the ACS at t≈.03 seconds. These plots show that the ACS significantly attenuated the instability. The middle plot compares the predicted and "observed" (by the ACS' observer) pressure oscillations. It shows that the developed observer can indeed "identify" the characteristics of the combustor pressure oscillations in practically real time. The second plot in the middle demonstrates the observer's ability to "follow" in real time the variations in the frequency of the instability. The plot on the bottom left presents an "amplified" view of the oscillations shown in the top left plot after activating the ACS. It shows that the amplitude of the "damped" combustor oscillations is negligible. Finally, the plot on the bottom right shows the time dependence of the control signal o the actuator. In summary, the results presented in Fig. 5 predict that the investigated ACS will effectively attenuate rocket motor combustion instabilities.

In a parallel study, Roe's Rieman Solver[3] was modified for applications in numerical simulations of unstable combustors. Specifically, Roe's Rieman scheme was modified to properly account for the presence of source terms (e.g., the combustion process heat addition, friction) in the numerical solution of the conservation equations. Furthermore, numerical schemes that improve the representation of the injector face and nozzle boundary conditions were developed for incorporation into the numerical solution scheme.

Finally, the feasibility of applying open loop, nonlinear, high frequency, vibrational control to damp instabilities in mechanical systems was theoretically investigated[4]. Such control has the advantage that it does not require accurate determination of the state of the controlled system and the data processing capabilities required in conventional feedback control. This paper extends previous linear investigations of this type of control to include nonlinear vibrational controllers. It shows that a nonlinear vibrational controller can stabilize a system even if the Jacobian matrix has a positive trace. A copy of this paper, which was submitted for publication in the IEEE Journal, is provided in Appendix.B.

Experimental Setup

The experimental efforts led to the development of an actively controlled, small scale, gas rocket motor setup shown in Fig. 6. It consists of a reactants feed system, a combustor section, a

nozzle, a secondary fuel injection system (i.e., the fuel injector actuator), a main control panel, and a computer-based controller of the secondary fuel actuator. The setup also includes transducers and photomultipliers that measure the combustor pressure and reaction rate, respectively, and a computer-based data acquisition system.

A primary reactants stream, consisting of premixed air and methane, enters the combustor through the injector orifices. The air and methane are separately introduced into a mixing port through calibrated, choked, orifices that provide means for measuring the flow rate of each reactant. These flow rates are manually controlled by setting the pressure upstream of each orifice to a desired value. The flows through the injector orifices are choked to prevent feedback between the combustor and reactants supply lines. The injected reactants jets are oriented twenty degrees relative to the combustor axis, which forces the primary combustion process to stabilize near the combustor walls.

The combustor's exhaust nozzle is choked at all test conditions. Under typical operating conditions, the combustor pressure, premixed reactants line pressure and fuel and air supply lines pressures are 45, 90 and 200 psi, respectively. The combustor pressure was always sufficient for choking the exhaust nozzle. The supply pressure to the secondary fuel injector is 450 psi. Under this operating condition, the flow rates of the primary stream of premixed fuel and oxidizer and secondary fuel stream are 10 and 0.1 gram/sec., respectively, resulting in a total combustor power output of 55 kW.

The combustor has a large length to diameter ratio to prevent excitation of transverse modes. The combustor length can be changed by adding or removing pipe sections. This capability permits the investigation of axial mode instabilities having different frequencies; high frequency instabilities are excited in short combustors and vice versa. At its shortest length, the combustor's fundamental mode frequency is around 1800 Hz. while at its longest configuration the fundamental mode frequency is 200 Hz. During operation, the combustor is immersed in a bath with running water to cool the combustor.

As shown in Fig. 6, the axis of the investigated combustor is "broken" to provide a location for installing the window, optics and photomultiplier required to measure the total (integrated) combustion zone radiation. This system measures the total CC or CH radicals radiation from the combustion region, which is proportional to the combustion process heat release rate. A second, side view, window, which is installed near the injector, is used for optical measurements and visualization of the combustion zone.

The actively controlled secondary fuel injector actuator introduces an oscillatory fuel flow into the combustion zone. High pressure fuel is supplied to the actuator and forced through an annular orifice between the outer wall of a needle's wider diameter base and its seat. A magnetostrictive actuator is attached to the needle and used to change the needle's base position relative to its seat in response to changes in an electric control signal. The acoustic impedance and pneumatic resistance of the actuator's cavities that carry the fuel from the supply line to the combustor were sized to maximize the fuel flow rate oscillations at the injector's exit and minimize the effect of the combustor pressure oscillations upon the actuator's performance over a wide frequency range. As a result, this actuator can modulate the fuel flow rate over a 0-1,200 Hz. frequency range when pressure oscillations are present in the combustor without a significant attenuation or a phase delay. Furthermore, this actuator can produce fuel flow rate amplitudes of the order of 0.2 grams/sec., which, in principle, can produce 20 kW peak to peak heat release rate oscillations.

The electric signal to the actuator consists of a steady and an oscillating component, which control the magnitudes of the steady and oscillating flow rates through the fuel injector actuator, respectively. Both signals are generated in the control computer, separately amplified, and then combined into a single control signal that is fed to the actuator.

Two different actuators and injection systems were developed and tested during this study. Each injection system, see Figs. 7-a,b, supplied the combustor with a primary stream of premixed reactants and a secondary fuel stream. The latter was used to control the instability by generating a secondary, oscillatory, combustion process within the combustor. The actuators were similar in design, but the annular cross sectional area of the second actuator was between two to three times larger than that in the first actuator. For further reference, the small and large actuators will be denoted as ACT1 and ACT2, respectively, and the injection systems shown in Figs. 7-a,b will be denoted by INJ1 and INJ2, respectively. The investigated injector/actuator configurations, whose performance is described later in this report, will be described by the notation INJi/ACTi where the index i=1,2 describes the injector and actuator used in the study. It should be pointed out that the ACT2 actuator, which was developed later in the program, could be retrofitted to both injection systems while the ACT1 actuator could be only installed on the INJ1 injector.

The second injector, INJ2, and actuator, ACT2, were developed and investigated in a cooperative effort with a major gas turbine manufacturer that is interested in developing capabilities for active control of instabilities in large scale gas turbines.

Open Loop Studies

As stated above, effective application of the investigated ACS in closed loop control of combustion instabilities requires knowledge of the gain and phase shift that the controller must add to each combustor unstable mode. Since each unstable mode oscillates at a different frequency and these frequencies may span a wide range, the frequency dependence of the phase shift and gain that the controller must add to the unstable modes must be known over a wide frequency range. Since, unfortunately, the characteristics of the secondary combustion processes cannot be accurately modeled to predict the frequency dependence of its phase shift and gain, these quantities must be experimentally determined in open loop tests. The objective of the open loop tests is to measure the phase delay between the combustion process heat release and actuator control signal oscillations and the ratio of the amplitudes of the combustion process heat release and control signal oscillations, which is referred to as the gain. Together, the measured phase shift and gain describe the secondary combustion process response (SCPR).

Another critically important reason for investigating the SCPR is to determine whether the developed fuel injector actuator can excite combustion process heat release and pressure oscillations within the combustor of sufficient magnitude (i.e., capable of affecting the unstable combustor oscillations) . If the developed fuel injector actuator could not excite heat addition oscillations of sufficient magnitude within the combustor, it would not be suitable for application in closed loop control of combustion instabilities. In this case, a different fuel injector (or another type of actuator) will have to be developed and/or investigated.

Two approaches for determining the SCPR frequency dependence were developed and investigated under this program. The first used a very short combustor whose fundamental, longitudinal, acoustic mode frequency was around 1800 Hz., which was significantly above the upper limit of the frequency range of the open loop studies. Consequently, the operation of the combustor was "quiet" over the investigated frequency range and the magnitudes of driven disturbances (by the fuel injector actuator) were significantly above the combustor noise level. When tests were conducted in this short combustor, high frequency reaction rate and pressure oscillations driven by a combustor instability could be readily observed in the measured pressure and radiation data and clearly distinguished from the "single" frequency oscillations driven by the fuel injector actuator. Using this combustor, the characteristics of the SCPR were determined from the measured pressure* and a relationship between these pressure oscillations and reaction rate

* Global radiation measurements could not be used with this combustor because the available sideview window, see Fig. 6, could not "view" the whole combustion zone.

oscillations, which was provided by a model of the combustor oscillations (which is derived below). The "short" combustor also included a side view window, similar to the one shown in Fig. 6, which was used to measure CH radicals radiation from the combustion region. Unfortunately, this window could not "view" the whole combustion region, and the measured radiation could only provide qualitative description of the characteristics of the secondary combustion process oscillations.

The following analysis describes the derivation of a model that predicts the behavior of small amplitude (i.e., linear) oscillations in the short combustor. This model was used to determine the SCPR from measured pressure data.

Neglecting kinetic energy terms, the energy equation for a combustor with uniform properties can be expressed in the following form:

$$\frac{d}{dt}\int_V \rho e dV = \dot{q}_{comb.} + \dot{m}_a h_a + \dot{m}_f h_f - \dot{m}_e h_e \qquad (6)$$

where the terms from left to right are the rate of change of the combustor internal energy, oscillatory heat release supplied by the secondary combustion process, the air and fuel enthalpy fluxes into the combustor and the enthalpy flux exiting through the choked nozzle, respectively. Assuming a perfect gas behavior and that the flow through the choked nozzle is quasi steady, the following relationships can be derived:

$$\frac{d}{dt}\int_V \rho e dV = (VC_v / R)\frac{dp}{dt}; \quad \dot{m}_e h_e = (K_N p / \sqrt{T})C_p T \qquad (7)$$

Substituting Eqs. (7) into Eq. (6), assuming that each dependent variable consists of a steady component and a small amplitude perturbation (e.g., $p = \bar{p} + p'$), and linearizing the resulting energy equation yields the following linear form of the energy equation

$$\frac{\dot{q}'}{\bar{\dot{m}} C_p \bar{T}} = \frac{p'}{\bar{p}} + \frac{\tau}{\bar{p}}\frac{dp}{dt} + \frac{T'_e}{2\bar{T}}; \quad \tau = \frac{VT_a\bar{p}}{\bar{T}C_a^2\bar{\dot{m}}} \qquad (8)$$

where τ is a characteristic time, C_a is the speed of sound and the subscript 'a' denotes the state of the incoming air. Since the temperature perturbations generated within the combustion process are expected to decay before they reach the nozzle entrance at high frequencies, the term involving T'_e is neglected in Eq. (8), yielding the following relationship

$$\frac{\dot{q}'}{\overline{\dot{m}} C_p \overline{T}} = \frac{p'}{\overline{p}} + \frac{\tau}{\overline{p}} \frac{dp}{dt} \qquad (9)$$

for determining the heat release $\dot{q}'$ oscillations from measured pressure oscillations at high frequencies.

In the second approach for determining the SCPR, the combustor shown in Fig. 6 was employed. Since this combustor is considerably longer than the "short" combustor that was used in the first study, several natural longitudinal acoustic modes of the combustor could be excited in the range of investigated SCPR frequencies. For example, the fundamental mode frequency of this combustor was 370 Hz. Consequently, small heat addition oscillations at one of the natural acoustic mode frequencies of the combustor could produce significant pressure oscillations at this frequency. Consequently, when the fuel injector actuator is operated at a non-resonant frequency of this combustor, it excites significant secondary combustion process oscillations within the combustor but only small amplitude pressure oscillations. Thus, the phase and amplitude of the secondary combustion process heat release oscillations can be determined at non-resonant frequencies of the combustor by direct measurements of the characteristics of the total radiation from the combustion region. These were directly measured with a photomultiplier through the window on the slanted combustor section in Fig. 6.

Figure 8 shows an example of the time dependence and spectra of pressure and CH radiation signals measured in the combustor shown in Fig. 8 when the secondary fuel injection rate oscillated at 610 Hz. Figure 8-a shows that the pressure spectrum is dominated by spikes representing three unstable combustor modes at 370, 740 and 1110 Hz. In general, if a single mode is driven by an unstable combustion process, the amplitudes of its harmonics, which are excited by nonlinear processes, are smaller than the amplitude of the most unstable lowest frequency mode. The pressure spectrum in Fig. 8-a indicates that this was not the case in this experiment as the amplitudes of the higher frequency spikes are larger than the amplitude of the fundamental mode. This suggests that each of the observed pressure oscillations was independently driven by the combustion process.

An examination of the pressure spectrum in Fig. 8 also shows a small, but clearly visible, spike at 610 Hz., the frequency of the actuator. In contrast, only one, large amplitude, spike is present in the spectrum of the CH radiation signal at 610 Hz. The dominance of the spike of the driven heat release oscillations in the CH radiation spectrum indicates that the fuel injector actuator could readily excite heat release oscillations in this combustor that are significantly larger than any

other heat release oscillation when the frequency of the fuel flow rate modulation was not close to any natural acoustic mode frequency of the combustor.

Figure 8 shows that FFT can be used to identify a small amplitude, periodic, pressure signal in the neighborhood of large amplitude spikes. It was found, however, that an FFT analysis cannot accurately determine the phase of such a small signal. Unlike the FFT determination of the amplitude, the FFT determination of the phase is highly sensitive to the frequency at which the FFT integral is evaluated. Since the FFT evaluation is performed at a discrete number of frequencies, it may not be performed at the exact frequency of the secondary combustion oscillations, thus increasing the likelihood of inaccurate phase determination.

To overcome the shortcomings of the FFT, a MATLAB-based software that employs an ensemble averaging technique was developed to accurately determine the amplitude and phase of the secondary heat release oscillations. The basic steps of this approach are:

1. The input to the actuator, (usually a current) is chosen as a reference signal.

2. Measured data points are correlated with the reference signal by referencing the time of each data point to a specific phase in the period of the reference signal, thus "collapsing" all the measured data points into one period.

3. A "moving" narrow-width window is used to obtain the ensemble average of the time dependence of the collected data over the period of the reference signal. It should be noted that the time dependence of the calculated average does not necessarily assume a sinusoidal shape.

4) The ensemble-averaged line is curve-fitted with a sinusoidal signal to obtain the corresponding amplitude and phase of the measured data.

Figure 9 presents typical results obtained with this data reduction approach, using the data presented in Fig. 8. The top to bottom plots on the left side of Fig. 9 show measured data points describing, respectively, the actuator control signal (current), actuator needle displacement, combustor pressure and combustion process CH radiation. The corresponding plots on the right side of Fig. 9 show the determined averages of the collected data points (solid lines) and the sinusoidal curves that were fitted to the ensemble-averaged curves (dashed lines).

The actuator current, pressure and CH radiation are measured by sensors with practically no time delay. In contrast, the proximity sensor that measures the actuator's needle displacement introduces a significant phase lag and attenuation to the measured data. This phase lag and attenuation, which are determined in advance by comparing known input signals at various

frequencies to the sensor's output, are accounted for in the data reduction procedure by providing the determined sinusoidal signal with a phase lead and a gain relative to the calculated "average" curve.

Figure 9 shows that the measured CH radiation and pressure data form "clouds" of points. While the CH radiation "cloud" exhibits a sine-like shape, such a pattern is not readily apparent in the thick "cloud" of pressure data points. This difference between the pressure and radiation data is reflected in the presence of high frequency components in the ensemble average of the pressure data, and the practically sinusoidal shape of the ensemble average of the CH radiation data, which nearly coincides with its sinusoidal curve fit.

The above described data reduction procedure was applied to the data measured in the open loop tests to obtain the frequency dependence of the phase and gain of the above described variables and, in particular, the transfer function between the needle displacement, which closely resembles the fuel injection modulation, and secondary combustion process heat release oscillations.

The frequency dependence of the gain and phase delay of the secondary combustion process heat release oscillations generated by the fuel injector actuator were measured by the two, above discussed, methods and the results are compared in Figs. 10-a,b. The excellent agreement between the two sets of data that were determined using different approaches in two different combustors strongly suggests that the frequency response of the heat addition oscillations generated by the developed fuel injector actuator is practically independent of the acoustic properties of the combustor.

Figures 11-a,b show the measured frequency dependence of the phase and gain of the secondary combustion process heat release of two different injector/actuator configurations that consisted of each of the developed injectors, see Figs. 7-a,b, and the larger fuel injector actuator (i.e., configurations INJ1/ACT2 and INJ1/ACT2). The frequency dependence of the SCPR of the INJ1/ACT2 configuration was determined for various magnitudes of the actuator's needle displacement. Figure 11-a shows that all the measured phase data can be closely correlated by a single curve that describes a nearly linear dependence of the phase upon the frequency. This nearly linear frequency dependence of the phase suggests the presence of a pure time delay between the fuel injection rate modulation and the corresponding secondary combustion process heat release oscillations. This is a surprising result as it was not expected that an identical, pure, time delay will be produced by different injectors and excitation levels.

Figure 11-b shows the frequency dependence of the ratio of the amplitudes of the combustion process heat release the actuator's needle displacement oscillations. Since these results apparently depend upon the amplitude of the needle's displacement, this amplitude is indicated next to some of the data points to provide means for determining the dependence of the data upon the needle's amplitude. Figure 11-b indicates that the INJ2 injector has a larger gain at frequencies below 300 Hz. and smaller gain at higher frequencies. It also shows that the gain depends upon the needle's displacement and is larger for smaller displacements. This result suggests that the SCPR is controlled by nonlinear processes whose potential origin is discussed below.

The developed fuel injector actuator provides the combustor with a fuel flow consisting of a mean and an oscillatory component. To maintain the mean flow rate at a set value, it is measured and compared with the set value. If the two are not equal, the mean flow rate controller sends a slowly varying signal to the actuator that changes the mean position of the needle and, thus, the mean area of the actuator's orifice, in an effort to provide the desired mean fuel flow rate. In addition to the slowly varying signal from the mean flow controller, the actuator receives a high frequency signal that sets the needle into high frequency, back-and-forth, axial oscillations that periodically vary the actuator's orifice cross sectional area, resulting in a periodic secondary fuel injection rate. As long as the periodic variation of the orifice's area is small and does not change its mean area, the periodic change in the orifice's cross sectional area does not interfere with the mean flow rate through the actuator. As the amplitude of the actuator's needle displacement oscillations increases, a threshold amplitude that forces the actuator's orifice to momentarily close (at the instant of maximum" upward" needle displacement, see Fig. 6) is reached. As the amplitude of the needle's displacement oscillations increases beyond this threshold value, the mean values of the actuator's needle displacement and mean flow rate increase, see Fig. 12. This forces the actuator's mean flow rate controller to further close the actuator orifice, resulting in additional "truncation" of the needle's oscillations. Since it can be shown that the amplitude of the actuator's orifice area variation oscillations cannot be larger than the magnitude the orifice's mean area, the amplitude of the fuel flow rate modulation cannot exceed that of the mean fuel flow rate.

Figure 13 shows the dependence of the ratio of the amplitude of the combustion process CH radiation oscillations and the mean CH radiation on the needle's displacement amplitude at a frequency of 540 Hz. for three different injector/actuator configurations. The behavior exhibited by the three plots is in agreement with the above discussion. They show that the amplitude of the CH radiation oscillations reaches a limiting value at a given needle displacement amplitude and cannot increase beyond this limiting value as the needle displacement is further increased.

To further understand the results of Fig. 13, we should consider the two main processes that control the interaction between the secondary combustion process heat release and needle displacement oscillations. First, consider the variation in the cross sectional area of the actuator's orifice, see Fig. 6, in response to the needle's displacement oscillations. As discussed above, the amplitude of the cross sectional area oscillations cannot exceed the mean magnitude of the cross sectional area of the orifice. Consequently, to increase the amplitude of the fuel flow rate modulation would require increasing the magnitude of its mean flow rate. The difference between the behavior of the two actuators that were used in this study is qualitative described in Fig. 14 where the expected dependence of the amplitude of the secondary fuel injection rate modulation upon the amplitude of the actuator's needle displacement is plotted for the large and small actuators operating with two different mean flow rates. Figure 14 shows that since the orifice of the larger ACT2 actuator has a larger cross sectional area than that of the ACT1, the ACT2 actuator provides larger amplitude fuel flow rate modulations for a given amplitude of the needle's displacement oscillations than the ACT1 actuator. It also shows that both actuators can provide the same maximum fuel flow rate oscillations amplitudes as long as they can provide the same fuel mean flow rate.

Another factor affecting the amplitude of the combustion process heat release oscillations is the "efficiency" of converting the secondary fuel injection rate modulations into combustion process heat release oscillations. Intuitively, one would expect that the ratio of the amplitudes of the combustion process heat release and secondary fuel injection rate oscillations would depend upon the injector design. Examining the configurations of the two investigated injectors, see Figs. 7-a,b, shows that injector INJ1 supplies the secondary fuel stream directly into the "center" of the primary combustion zone whereas injector INJ2 apparently injects the secondary fuel upstream of the primary combustion region, possibly enabling the secondary fuel to fully or partially mix with the premixed, primary, reactants before reaching the combustion zone. This pre-mixing process apparently tends to decrease the magnitude of the attained secondary combustion heat release oscillations. Consequently, injector INJ1 is expected to provide a more "efficient" conversion of the fuel injection rate modulation into combustion process heat release oscillations than injector INJ2.

On the basis of the above discussion, one would expect that configurations INJ1/ACT2 and INJ2/ACT1 will produce the largest and smallest secondary combustion process heat release oscillations for a given needle displacement, respectively, while configurations INJ1/ACT1 and INJ2/ACT2 will produce heat release oscillations that fall between these limits. These expectations are supported by the results in Fig. 13, where it is shown that for a given amplitude of the

actuator's needle displacement the amplitude of the secondary heat release oscillations decreased in the following order: INJ1/ACT2, INJ1/ACT1 and INJ2/ACT2.

The above discussion and Figs. 13 and 14 indicate that the smaller ACT1 actuator could provide the same maximum fuel flow rate and heat release oscillations as the larger ACT2 actuator if it could be provided with a larger maximum needle displacement amplitude. This explains why the two configurations INJ1/ACT1 and INJ1/ACT2 that used the same injector but different actuators attained the same maximum secondary heat release magnitudes, see Fig. 13. It is also interesting to note in Fig. 13 that the maximum amplitude of heat release oscillations that can be excited by the INJ2 injector is significantly smaller than those excited with the INJ1 injector even though INJ2 used the larger ACT2 actuator.

Closed Loop Active Control of Instabilities

As stated earlier, the investigated ACS is guided by Rayleigh's criterion and its objective is to generate heat addition oscillations within an unstable combustor 180 degrees out of phase with the unstable pressure oscillations. This mode of control will be discussed assuming that the instability can be damped by controlling its dominant mode only. In this case, the observer only identifies the dominant mode and the control signal to the actuator, y_c, is given by:

$$y_c = G(\omega) \bullet \left(S \cdot \sin(\omega t + \phi(\omega)) + C \cdot \cos(\omega t + \phi(\omega))\right) \qquad (10)$$

where S, C and ω are the observed amplitudes and frequency of the dominant mode while G(ω) and ϕ(ω) are the gain and phase that are added by the controller using data (in the form of plots or tables) obtained in the above discussed open loop experiments. Since Fig. 10-b shows that the gain of the heat addition oscillations decreases with increasing frequency, the magnitude of G(w) should increase with frequency to assure that the ACS generates heat addition oscillations of adequate magnitude at higher frequencies.

Closed loop control of the rocket motor setup shown in Fig. 6 was investigated. Combustor pressure, control signal and observed frequency measured in a typical test before and after activation of the ACS are described in Fig. 15. In this experiment, the development of a large amplitude instability was "monitored" by the observer before activating the control system at t=0.1 seconds. The ACS was "conditionally" activated by requiring the gain G(ω) in Eq. 10 to satisfy the following conditions

$$G(\omega) = \begin{cases} 0 & when \ \ |\omega_{observed} - \omega_0| > d_1 = 100\,Hz. \\ \\ G_{table} & when \ |\omega_{observed} - \omega_0| < d_2 = 50\,Hz. \end{cases} \qquad (11)$$

where ω_0 is the observed frequency of the instability before activating the controller (see Fig. 15) while d_1 and d_2 are specified parameters. These conditions require the controller to "remember" the frequency of the dominant unstable mode before activating the ACS and to respond only when this mode becomes dominant, thus leaving other modes uncontrolled. This mode of operation demonstrates the high flexibility of the developed control approach.

Figure 15-a shows that this ACS practically damped the instability in 40 milliseconds, indicating that it could damp rocket instabilities before they could seriously damage the engine and/or result in mission failure. FFT analysis of the combustor pressure oscillations before and after the activation of the ACS showed that the amplitude of the dominating mode was reduced by 26 dB., which exceeds the performance of ACS investigated elsewhere (see survey of results in Table 1 in Ref. 5). Figure 15-b describes the time dependence of the control signal to the actuator, which is proportional to the magnitude of $G(\omega)$ (see Eqs. 10 and 11) and, thus, depends upon the observed frequency, see Fig. 15-c. Figures 15-b,c show that the control signal goes to zero when the 370 Hz. dominant mode is damped by the ACS. When this occurs, the observer identifies the 740 Hz. harmonic as the dominant mode and stops controlling the 370 Hz. mode, see Fig. 15-b. Consequently, the unstable 370 Hz. mode starts growing again. When its amplitude exceeds that of other unstable combustor modes (e.g., the 740 Hz. mode), the observer identifies this mode again as the dominant mode and turns on the actuator. As shown in Figs. 15-b,c, this sequence of events continuously repeats itself, resulting in effective control of the dominant 370 Hz. mode, while not destabilzing other modes of the combustor.

Additional closed loop experiments, not reported herein, have demonstrated that the investigated ACS can effectively control multi-mode instabilities.

Summary and Conclusions

In closing, this report presents a novel active control approach for damping detrimental rocket instabilities. The main contributions of this study are:

1. the development of an active control approach based upon Rayleigh's criterion,

2. the development and demonstration of an observer that can determine the amplitudes, phases and frequencies of a prespecified number of unstable, combustor modes in real time,

3. the development of theoretical models for investigating active control of linear and nonlinear instabilities in rocket motors,

4. the development of a fuel injector actuator that utilizes a magnetostrictive material to modulate a secondary fuel injection rate over a 0-1,200 Hz. range, which is wider than that of any known injector,

5. the demonstration that the developed fuel injector actuator can excite significant reaction rate heat release oscillations within the combustor,

6. the development of two different approaches for determining the frequency dependence of the response of the secondary combustion process generated by the fuel injector actuator, and

7. the demonstration that closed loop application of the investigated ACS significantly (e.g. by 26 dB.) and rapidly (e.g., within 40 milliseconds) damps a rocket motor instability without destabilization of any stable modes.

It is believed that these findings provide a foundation for guiding the development of ACS for unstable rockets and other combustors.

References

1) Neumeier, y. and Zinn, B. T. Active Control of Combustion Instabilities Using Real Time Identification of Unstable Combustor Modes. Proceeding of 4th IEEE Confeerence on Control Aplication. Sept. 28-29, 1995, Albany, N.Y.

2) Neumeier, y. and Zinn, B. T. Active Control of Combustion Instabilities With Real Time Observation of Unstable Combustor Modes. AIAA 96-0758, 34th Aerospace Sciences Meeting, Jan. 15-18, 1996, Reno, NV. (submitted to AIAA Journal of Propulsion and Power)

3) Mohanraj, R., Neumeier, Y. and Zinn, B. T., Modification of Roe's Riemann Solver for the Euler Equations with Source Terms. AIAA 96-0766, 34th Aerospace Sciences Meeting, Jan. 15-18, 1996, Reno, NV.

4) Shapiro, B. and Zinn B. T. High Frequency Nonlinear Vibrational Control. Submitted to IEEE Transaction on Automatic Control.

5) Sivasegaram, S., Tsai, R. F. and Whitelaw, J. H. Control of Combustion oscillations by Forced Oscillation of Part of the Fuel Supply. Combust. Sci. and Tech. 1995 Vol. 105, pp. 67-83

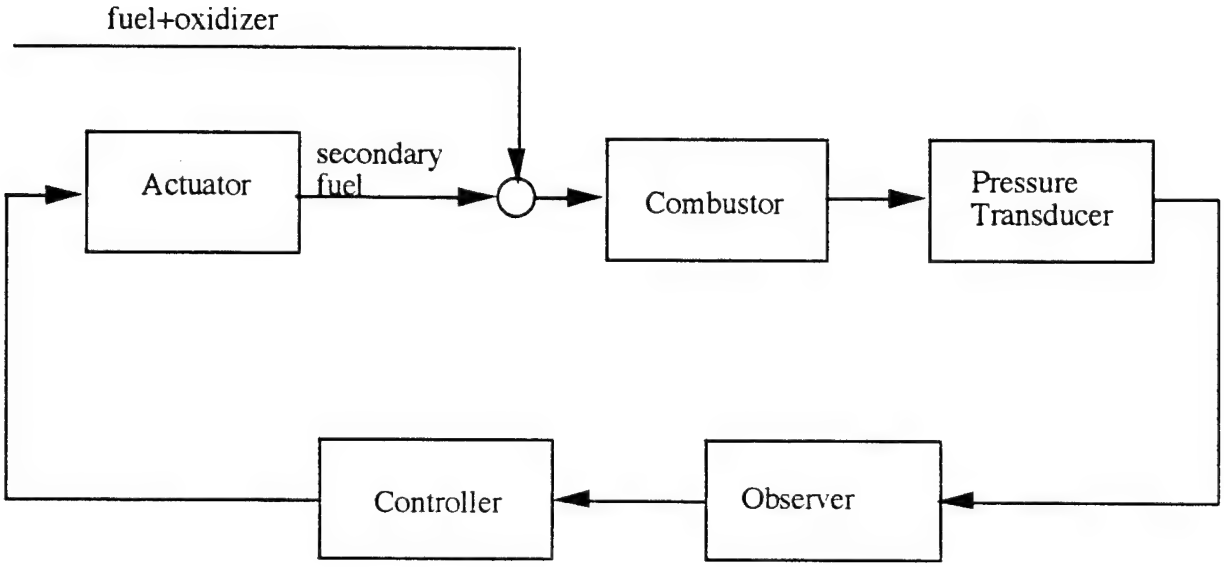

Figure 1. A schematic of the developed ACS.

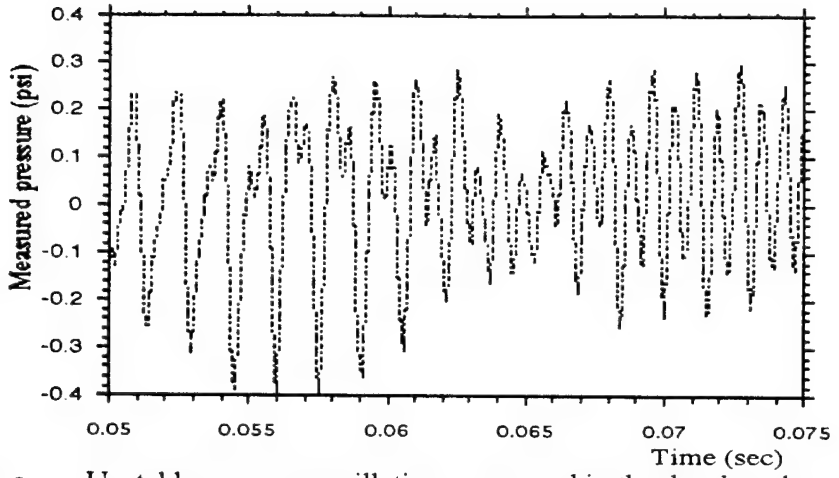

Figure 2-a. Unstable pressure oscillations measured in the developed gas rocket motor.

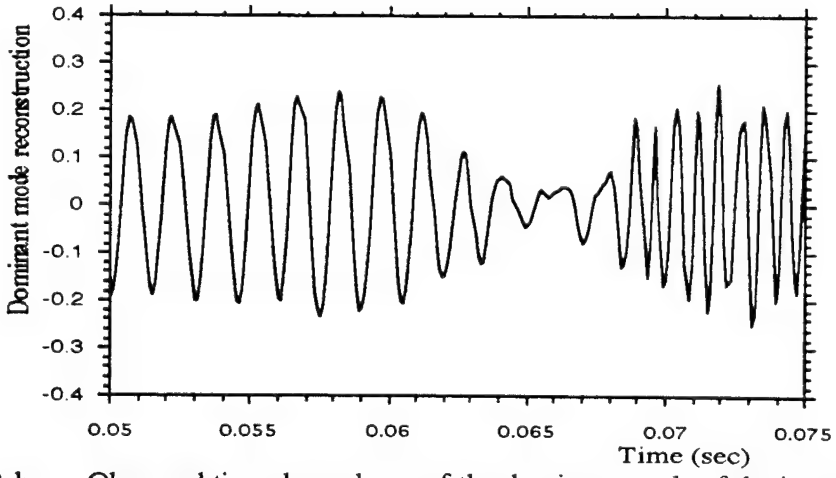

Figure 2-b. Observed time dependence of the dominant mode of the instability.

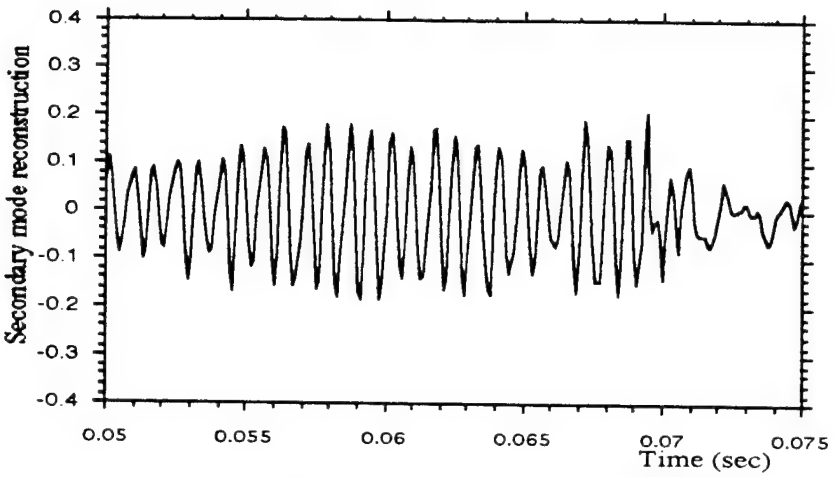

Figure 2-c. Observed time dependence of the secondary mode of the instability.

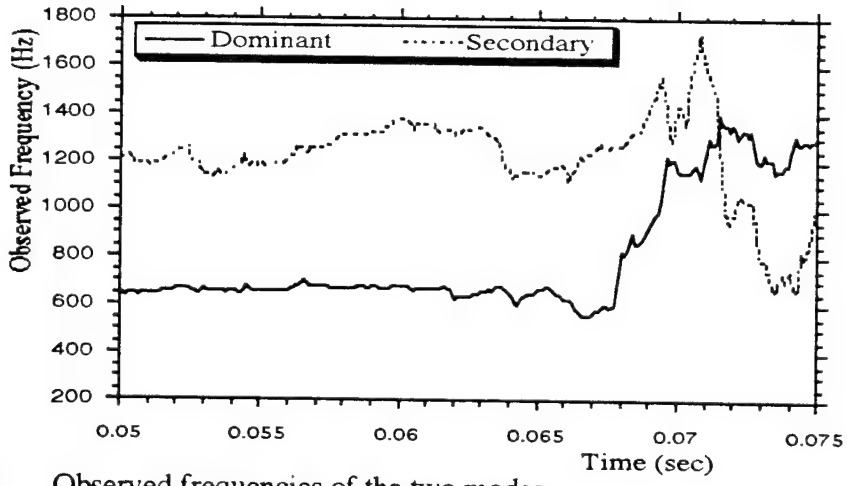

Figure 2-d. Observed frequencies of the two modes.

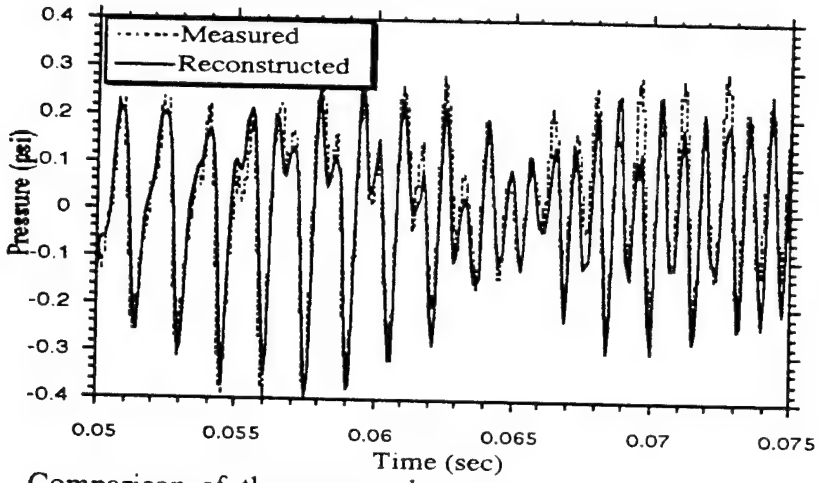

Figure 2-e. Comparison of the measured pressure and that synthesized from two observed modes.

$$\frac{\partial U}{\partial t} = -\frac{\partial F}{\partial x} + \eta(x)\left(\frac{U_{mix} - U}{\tau_{mix}}\right) + S \qquad U = \left\{\rho, \rho u, \rho\left(e + \frac{u^2}{2}\right)\right\}^T$$

$$F = \left\{\rho u, \rho u^2 + p, \rho u\left(h + \frac{u^2}{2}\right)\right\}^T \qquad e = \frac{p}{(\gamma - 1)\rho} \qquad h = \frac{\gamma p}{(\gamma - 1)\rho}$$

$$U_{mix} = \frac{\int_{V_{mix}} U\eta dV}{\int_{V_{mix}} \eta dV} \qquad S = (s_1, s_2, s_3)^T$$

$$\frac{\partial \rho_f}{\partial t} = -\frac{\partial[\rho_f u]}{\partial x} + \eta(x)\left(\frac{\rho_{f,mix} - \rho_f}{\tau_{mix}}\right) + \omega_f + s_f$$

$$\frac{\partial \rho_{ox}}{\partial t} = -\frac{\partial[\rho_{ox} u]}{\partial x} + \eta(x)\left(\frac{\rho_{ox,mix} - \rho_{ox}}{\tau_{mix}}\right) + \omega_{ox}$$

Reaction rate model (Global Kinetics)

$$\omega_f = \omega_{CH_4} = -2.15 \times 10^{16}\left[\rho_{CH_4}\right]^{0.2}\left[\rho_{O_2}\right]^{1.3} e^{\left[\frac{-24,368}{T}\right]}$$

Heat release

$$\dot{q} = -Q_{cal}\omega_f$$

Weighting function

$$\eta(x) = e^{-(x - x_f)/l_{mix}} \qquad x \geq x_f$$
$$= 0 \qquad x < x_f$$

U_{mix}	Weighted average of the state vector
s_1, s_2, s_3	Source terms due to secondary mass, momentum and heat addition
s_f	Source term due to secondary (controller) fuel addition
$\dot{q}$	Heat release due to chemical reaction (s_3 contains $\dot{q}$)
Q_{cal}	Calorific value of the fuel (methane)
x_f	Flame holder location
l_{mix}	Characteristic mixing length

Figure 3. Conservation equations used to model the behavior of an unstable gaseous rocket motor.

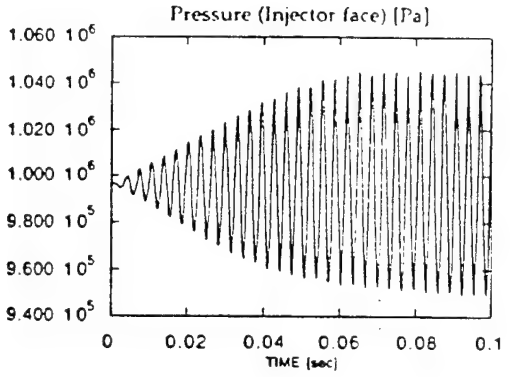

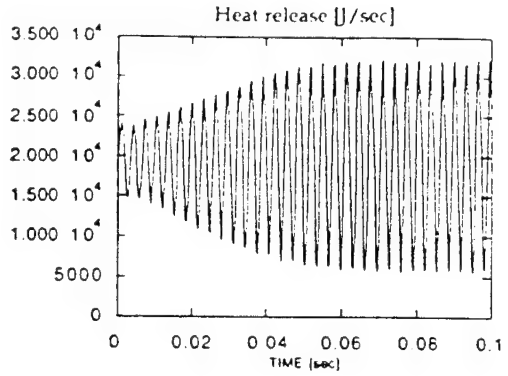

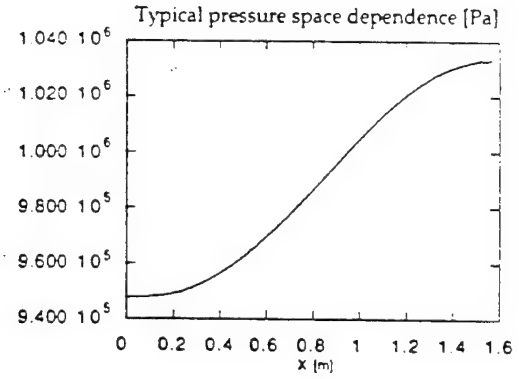

$L_{chamber}$=1.57 m
τ_{mix}=0.3 ms
l_{mix}=4 cm
x_f=2 cm
x_{secf}=2 cm
ϕ=0.7 (equivalence ratio)
Secondary fuel constitutes 40% of the total fuel.

Phase difference between heat release and pressure (heat release leading pressure)
28^0 (around t=0) and 71^0 (around t=0.1sec)

Figure 4. Prediction of the combustor response to open loop excitation by oscillatory fuel injection.

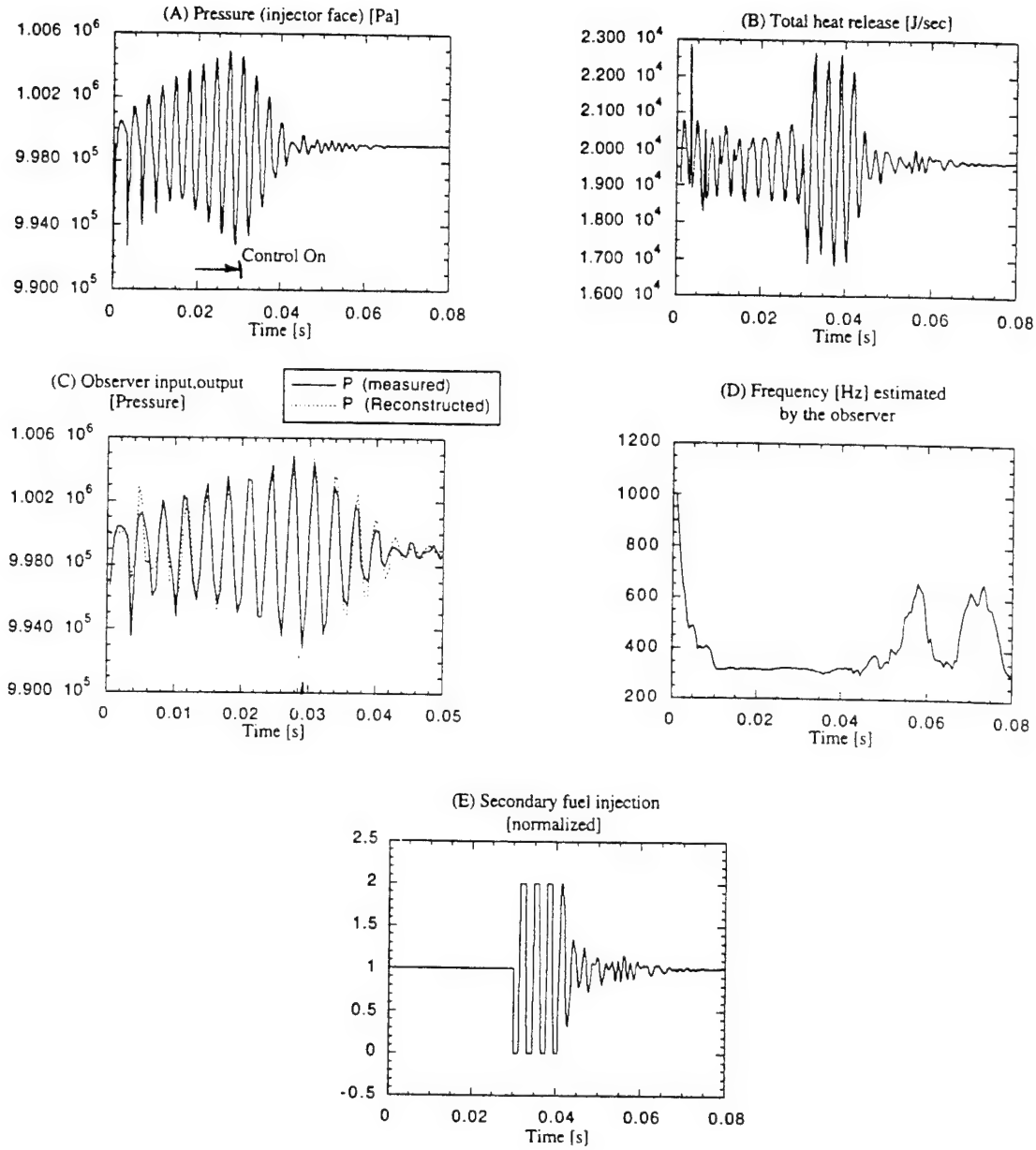

Figure 5. Results of numerical simulation of an unstable combustor response to closed loop active control by means of an oscillatory secondary fuel injection using real time observation of the dominant mode.

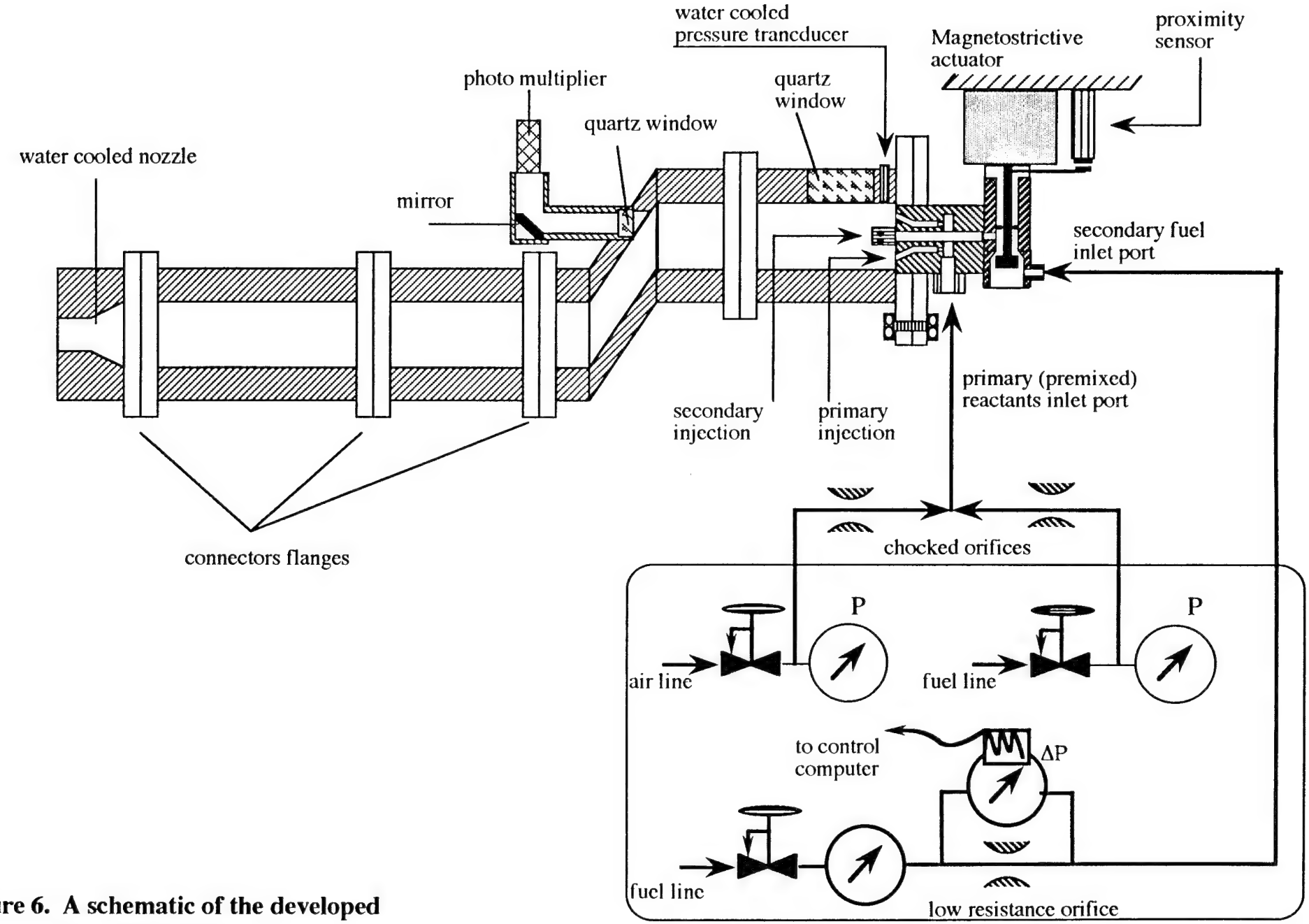

Figure 6. A schematic of the developed gas rocket setup

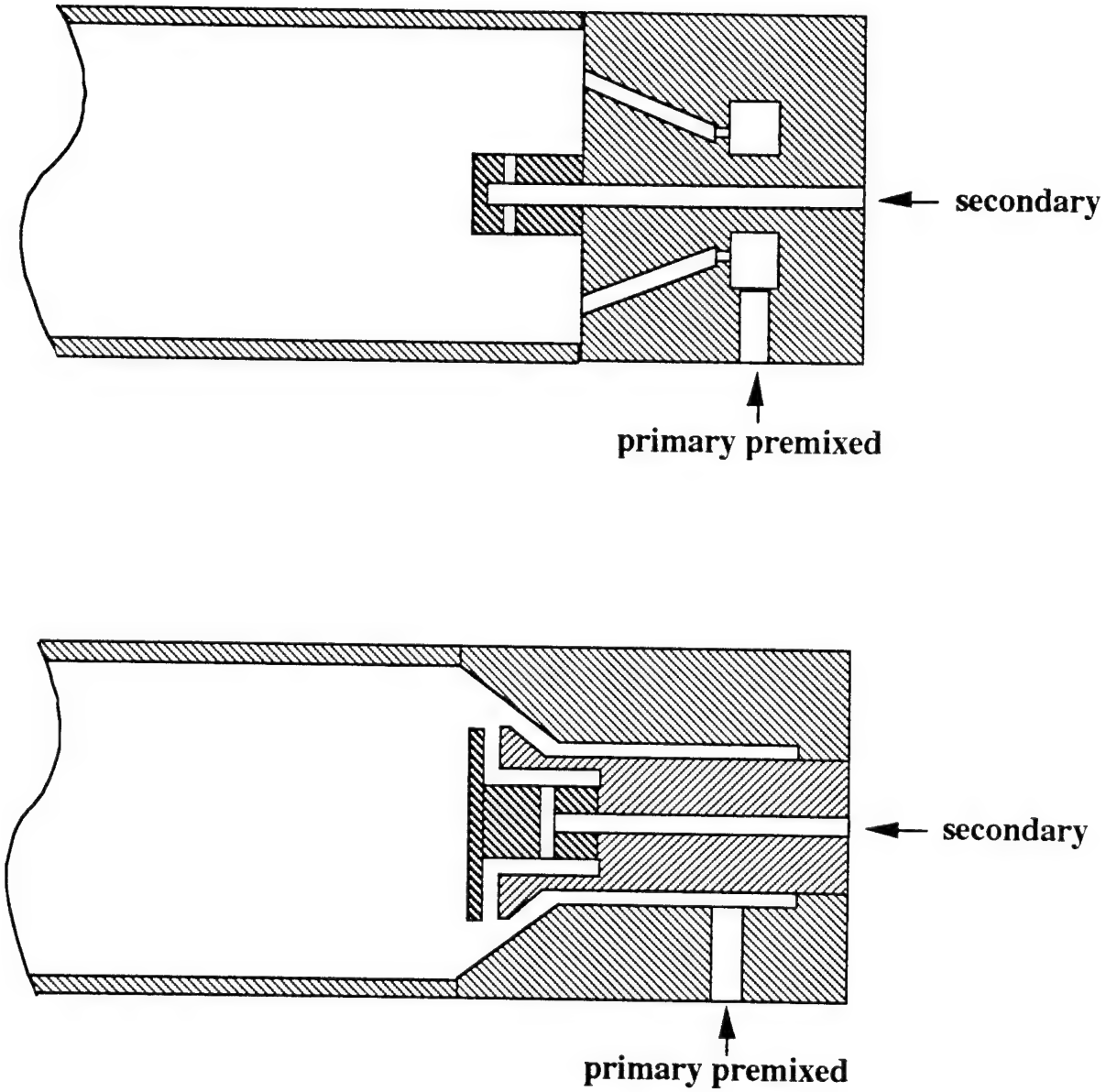

Figure 7. A schematic of the investigated, INJ1 (above) and INJ2 (below), injectors.

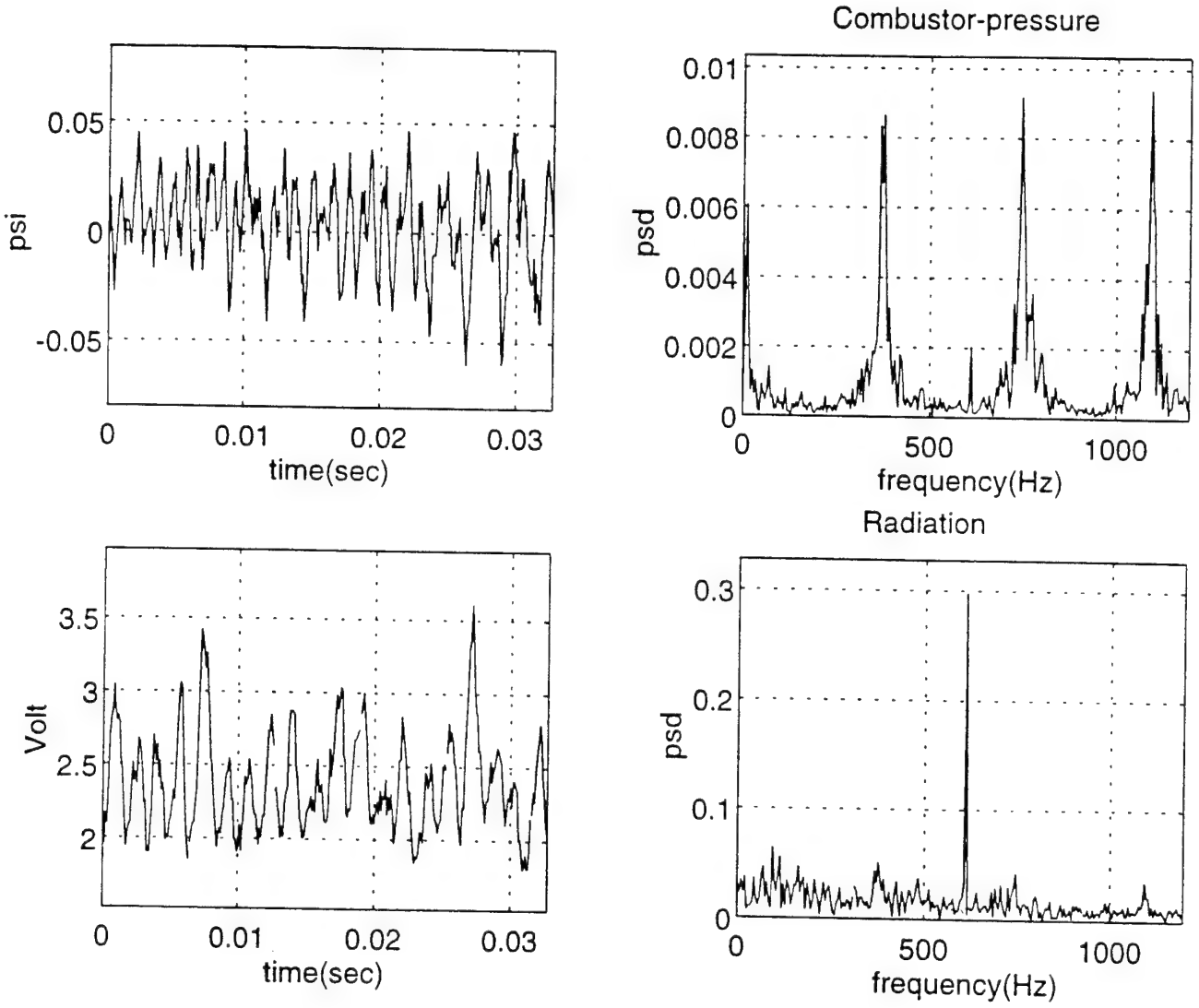

Figure 8. Time dependence and spectra of the combustor pressure and combustion region CH radicals radiation measured in an open loop experiment.

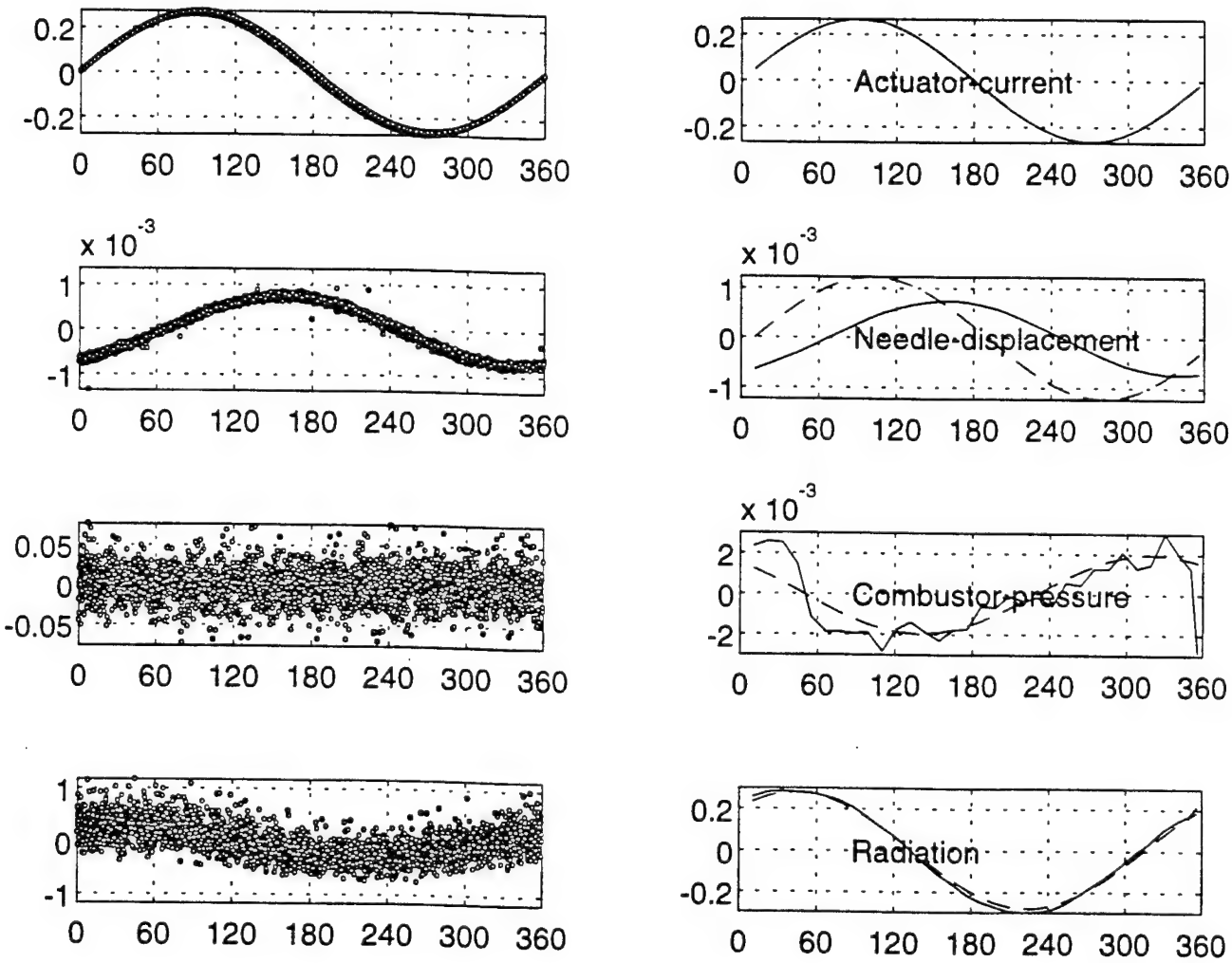

Figure 9. Measured and ensemble averaged data describing the actuator current, needle displacement, combustor pressure and CH radicals radiation obtained in the open loop experiment whose results are presented in Fig. 8.

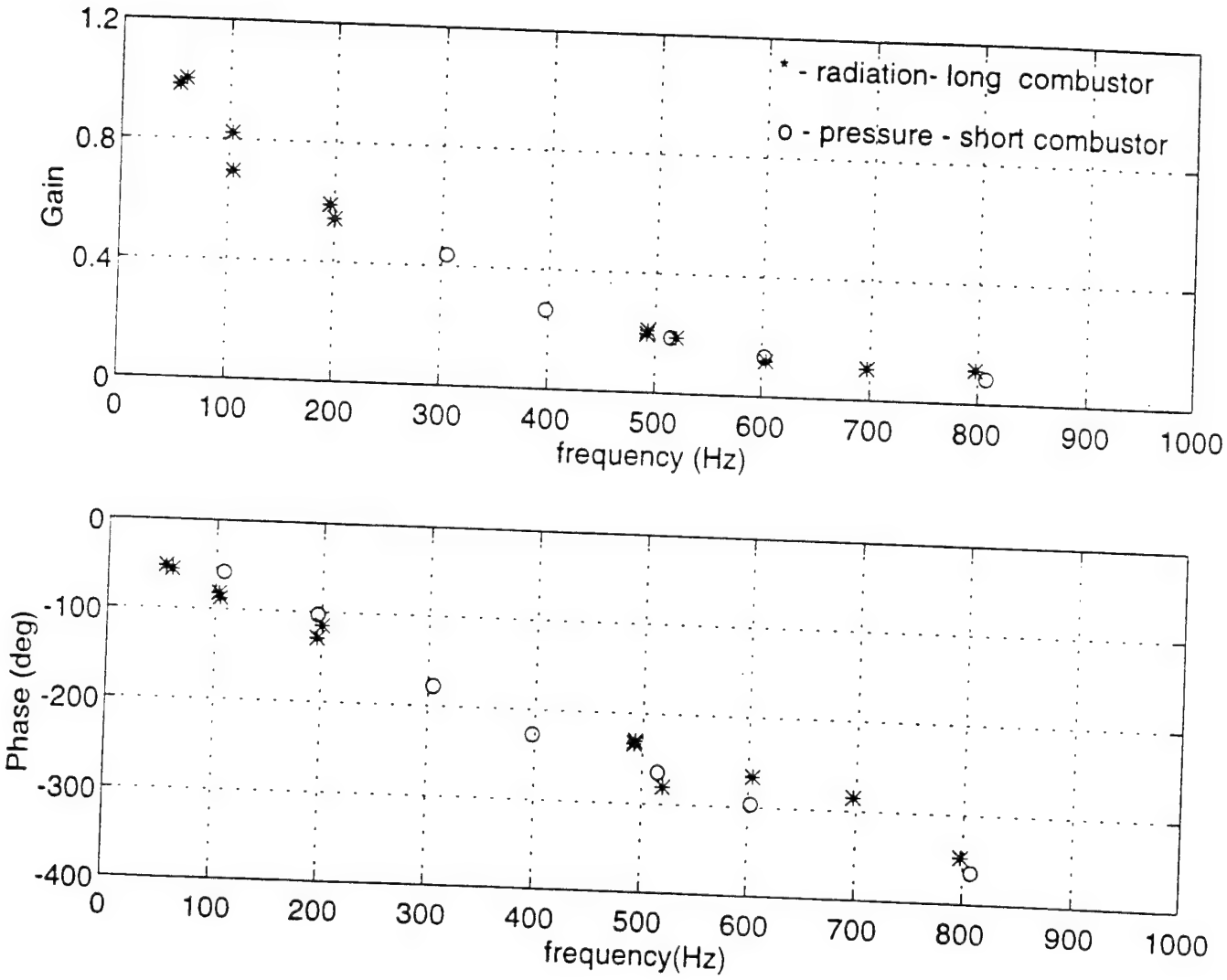

Figure 10. Comparisons of the frequency dependence of the amplitude and phase of the heat release oscillations produced by the fuel injector actuator obtained using pressure data measured in the short combustor and direct CH radiation measurements in the long combustor.

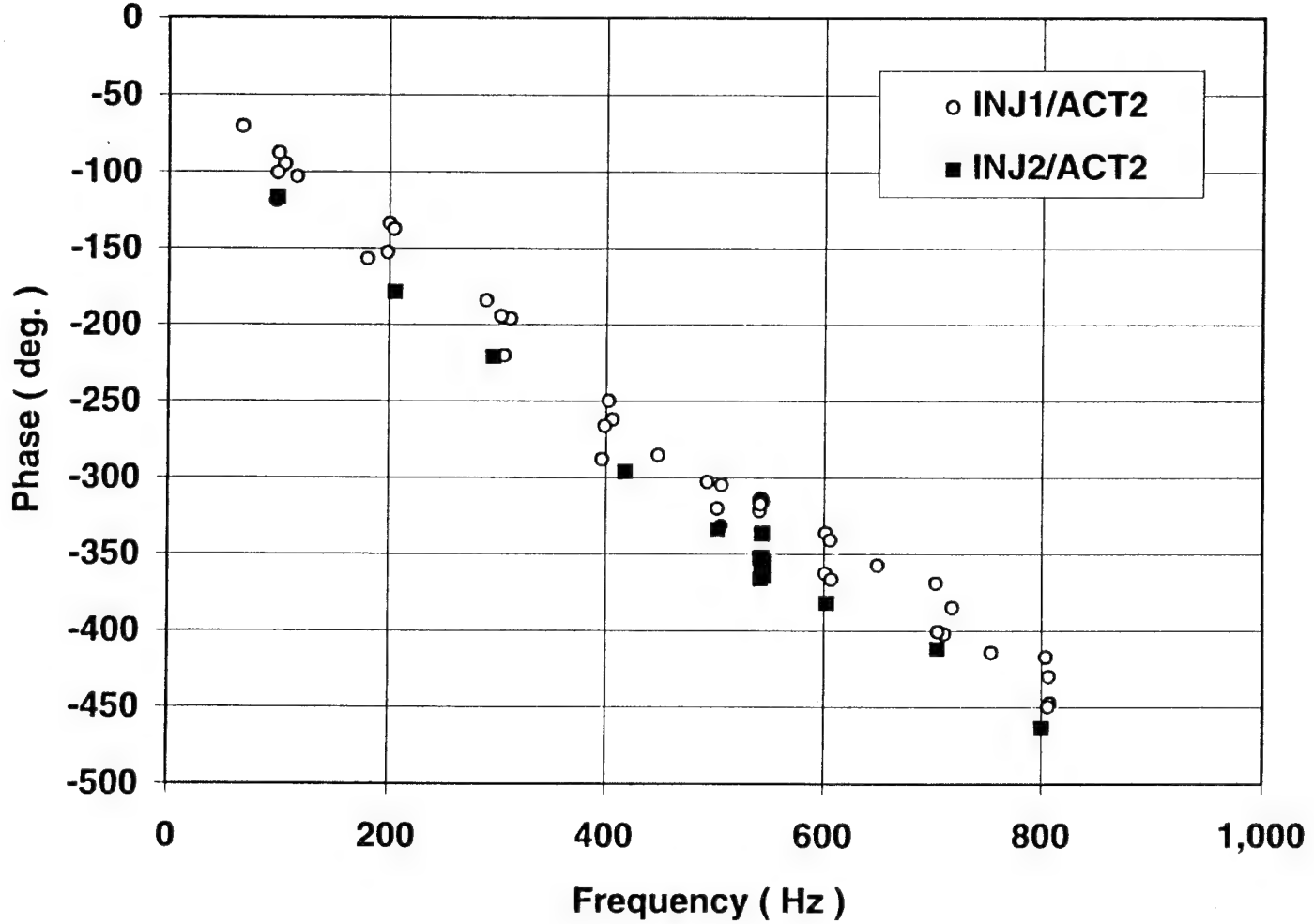

Figure 11-a. Phase difference between heat release and actuator displacement oscillations for two different injector/actuator configurations.

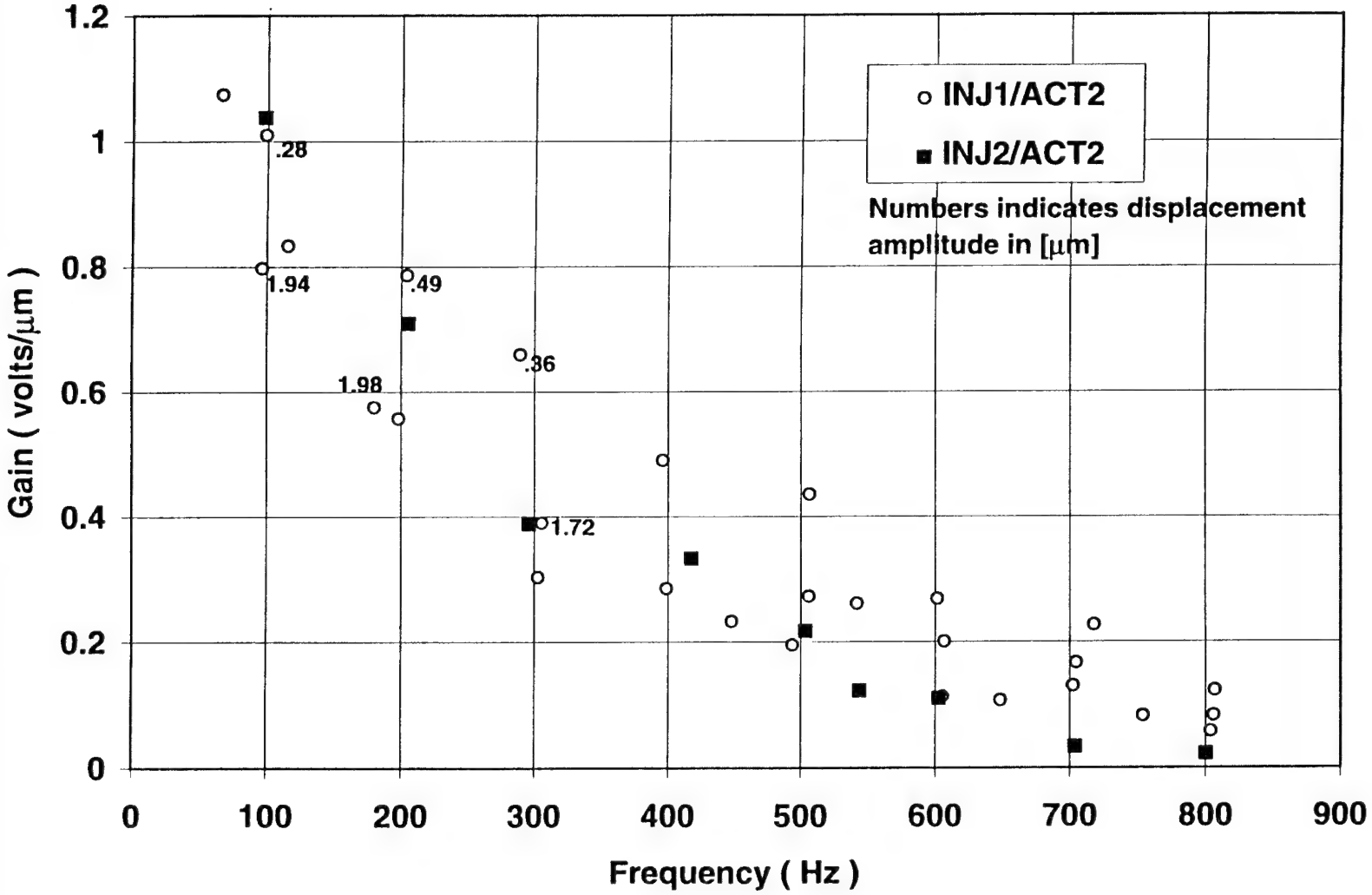

Figure 11-b. Gain of heat release with respect to actuator displacement oscillations for two different injector/actuator configurations.

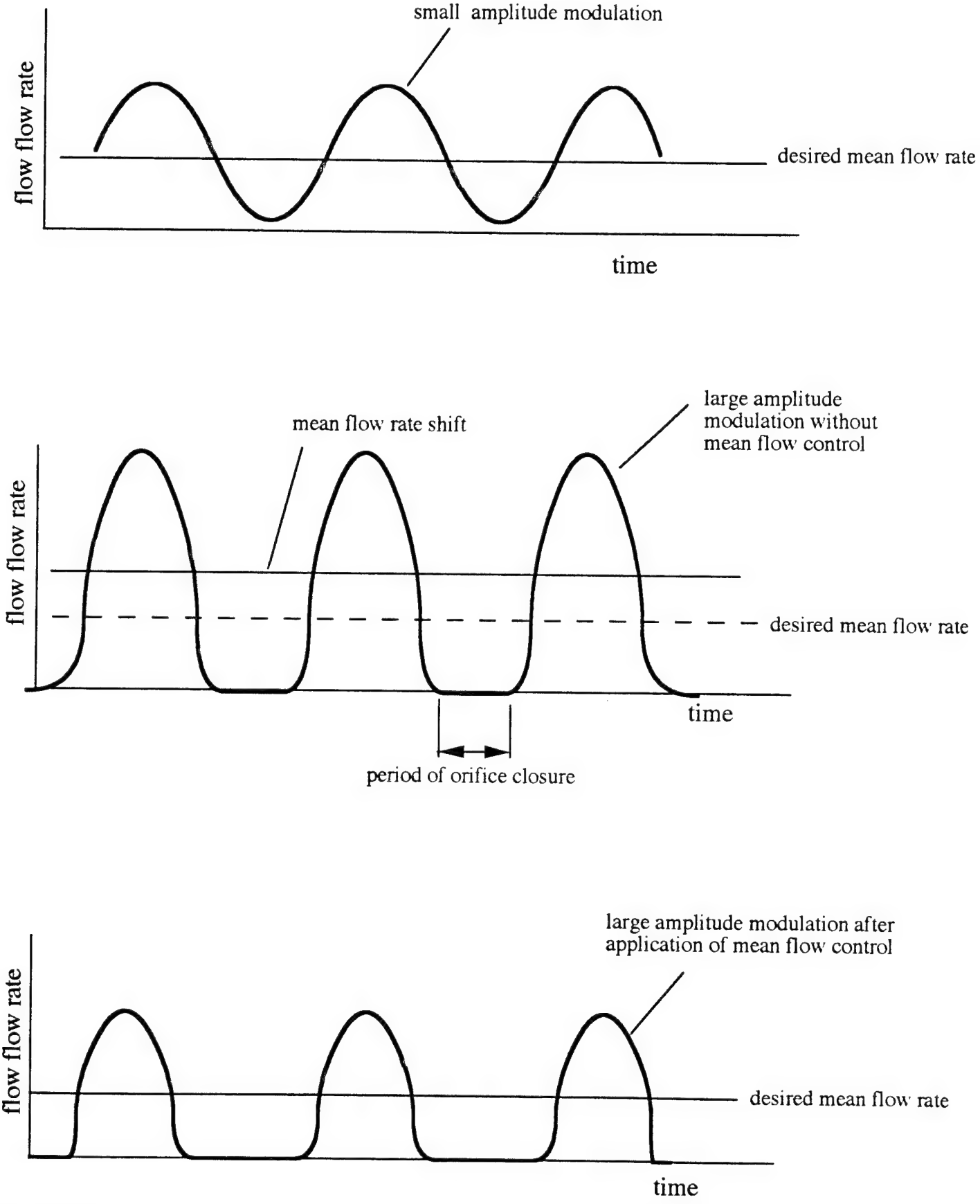

Figure 12. Qualitative description of the effect of mean flow control upon fuel flow modulation

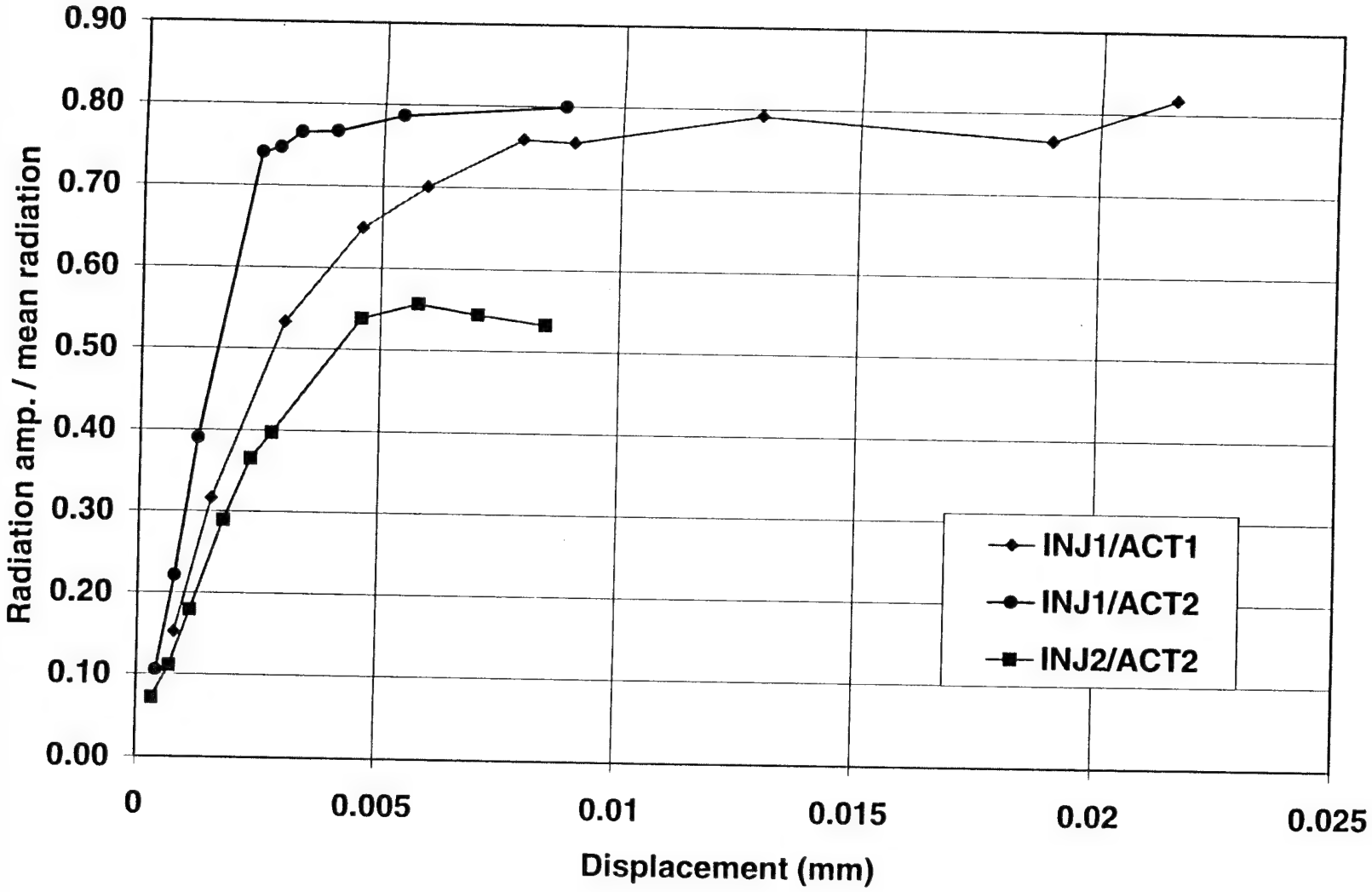

Figure 13. The dependence of the ratio of oscillating to mean heat release radiation upon the displacement of the actuator's needle amplitude.

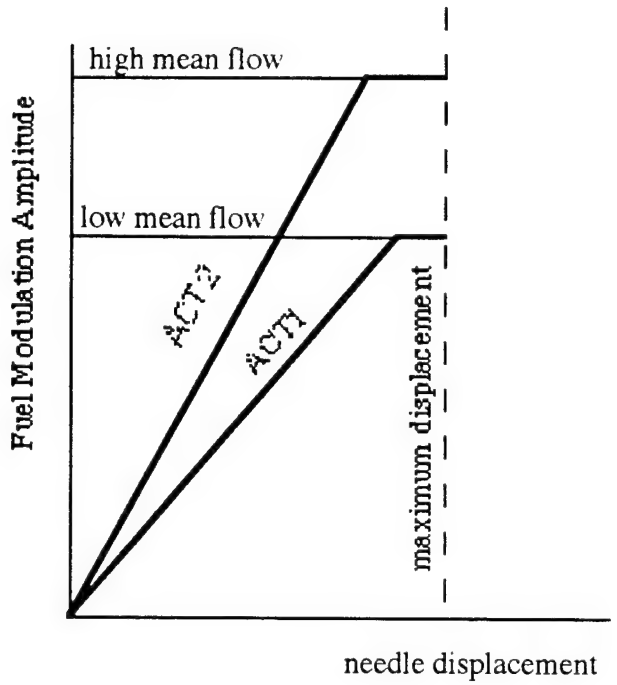

Figure 14-a. Qualitative description of the dependence of the fuel modulation amplitude upon the needle displacement amplitude for two different actuators and mean flows.

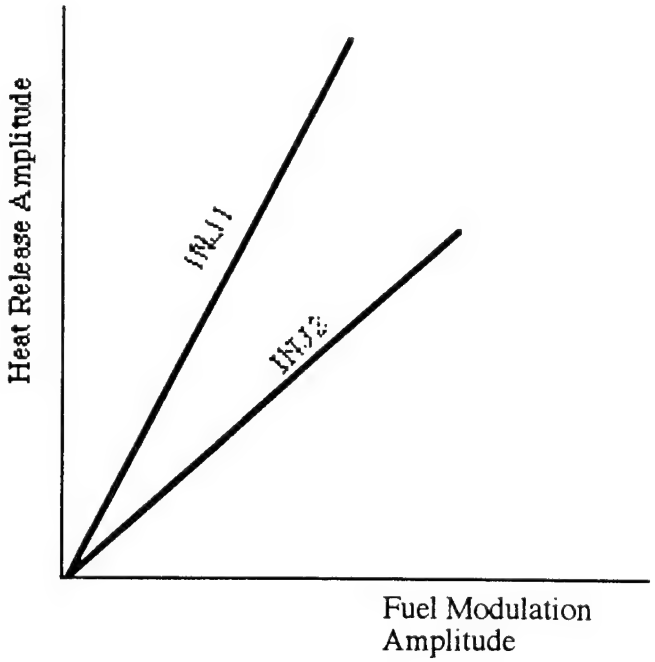

Figure 14-b. Qualitative description of the dependence of the heat release amplitude upon the amplitude of the fuel flow modulation for two different injectors.

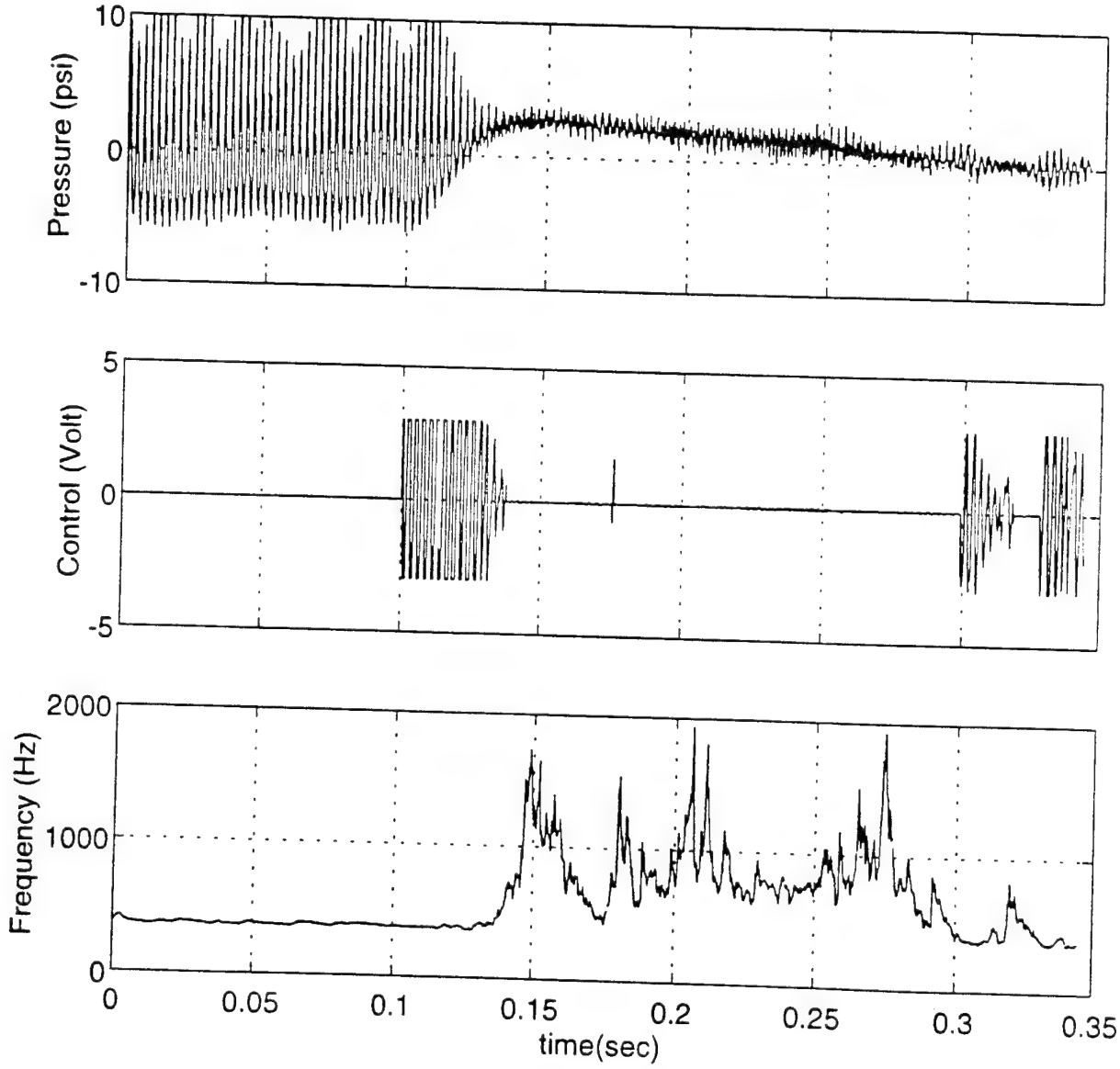

Figure 15. Time dependence of the pressure, control signal and observed frequency before and after the activation of the ACS in the gas rocket .

Appendix A

Extension of the Theory of the Observer for Simultaneous Identification of an Arbitrary Number of Modes in the Input Signal

Prepared by

Nikos Markopoulos and Yedidia Neumeier

1. Introduction

The frequency adaptation formula used so far in our observer is based on a single, sinusoidal input. If we know a signal at each instant of time, and if we also know that the signal is indeed a sinusoid, then, this frequency adaptation formula supplies us with the exact frequency of the sinusoid, without the need for any iterations. In practice, the need for iterations arises because of at least two reasons. First, the real pressure signals that we encounter in a combustion chamber vary with time in a manner that is far more complex than that of a single sinusoid. Second, the frequency domain characteristics of such signals are not stationary, but change, at best slowly, with time. We may be able to improve this situation at least partially by generalizing our frequency adaptation formula, so that it is accurate for input signals that are composed of an arbitrary number of sinusoids. Then, by accounting for a large enough number of sinusoids, we hope to increase the accuracy and ease with which we capture the characteristics of real signals exhibiting a discrete energy spectrum. This in turn may make our observer more robust and reduce some of our worries about convergence. This generalization of the frequency adaptation formula is given here in two steps. First, in Section 2, the formula is generalized to an input signal that is equal to a sum of two sinusoids. Then, with the insights gained in Section 2, the formula is generalized in Section 3 to an input signal that is equal to a sum of an arbitrary number of sinusoids.

2. Extending the Theory of the Observer to two modes

2.1 The input signal

Consider a signal f(t) given by:

$$f(t) = f_1(t) + f_2(t) \tag{1}$$

where $f_1(t)$ and $f_2(t)$ are two sinusoids:

$$f_1(t) = C_1 \sin \Omega_1 t + D_1 \cos \Omega_1 t \tag{2}$$

$$f_2(t) = C_2 \sin \Omega_2 t + D_2 \cos \Omega_2 t \tag{3}$$

Assume that:

(i) We know f(t) at each instant of time t.

(ii) We know that f(t) is a sum of two sinusoids.

The problem that we will try to solve is the following: Based on the information given in (i), (ii), determine the characteristics of f(t), that is, the frequencies Ω_1 and Ω_2, and the amplitudes C_1, D_1, C_2, and D_2.

2.2 The observer

To solve the problem, in analogy with the one-mode case, we set up an "observer" signal F(t) in the following way: F(t) is equal to the sum:

$$F(t) = F_1(t) + F_2(t) \tag{4}$$

with $F_1(t)$ and $F_2(t)$ given by:

$$F_1(t) = A_1(t)\sin\omega_1 t + B_1(t)\cos\omega_1 t \tag{5}$$

$$F_2(t) = A_2(t)\sin\omega_2 t + B_2(t)\cos\omega_2 t \tag{6}$$

Here ω_1 and ω_2 are two arbitrary frequencies that we select in advance for our observer. The time functions $A_1(t)$, $B_1(t)$, $A_2(t)$, and $B_2(t)$ are given by:

$$A_1(t) = \frac{2}{T_1}\int_{t-T_1}^{t}[f(\tau) - F_2(\tau)]\sin\omega_1\tau\, d\tau \tag{7}$$

$$B_1(t) = \frac{2}{T_1}\int_{t-T_1}^{t}[f(\tau) - F_2(\tau)]\cos\omega_1\tau\, d\tau \tag{8}$$

$$A_2(t) = \frac{2}{T_2}\int_{t-T_2}^{t}[f(\tau) - F_1(\tau)]\sin\omega_2\tau\, d\tau \tag{9}$$

$$B_2(t) = \frac{2}{T_2}\int_{t-T_2}^{t}[f(\tau) - F_1(\tau)]\cos\omega_2\tau\, d\tau \tag{10}$$

In Eqs. (7-10) $T_1=2\pi/\omega_1$ and $T_2=2\pi/\omega_2$ are the periods corresponding to the observer frequencies. Using some well-known trigonometric identities, we can completely eliminate $A_1(t)$, $B_1(t)$, $A_2(t)$, and $B_2(t)$ and work directly with $F_1(t)$ and $F_2(t)$. Combining Eqs. (5), (7), and (8) one obtains:

$$F_1(t) = \frac{2}{T_1}\int_{t-T_1}^{t}[f(\tau) - F_2(\tau)]\cos\omega_1(t-\tau)\, d\tau \tag{11}$$

Similarly, combining Eqs. (6), (9), and (10) results in:

$$F_2(t) = \frac{2}{T_2}\int_{t-T_2}^{t}[f(\tau) - F_1(\tau)]\cos\omega_2(t-\tau)\, d\tau \tag{12}$$

Our observer is completely described by Eqs. (4), (11), and (12). If one thinks of $F_1(t)$ and $F_2(t)$ as the estimates of $f_1(t)$ and $f_2(t)$ respectively, then, from Eq. (11), the input for evaluating the estimate of $f_1(t)$ is f(t) minus the estimate of $f_2(t)$. Likewise, from Eq. (12), the input for evaluating the estimate of $f_2(t)$ is f(t) minus the estimate of $f_1(t)$. The symmetry is complete.

For the particular f(t) given by Eqs. (1-3), the solution of Eqs. (11-12) can be expressed as:

$$F_1(t) = F_{11}(t) + F_{12}(t) \tag{13}$$

where $F_{11}(t)$ and $F_{12}(t)$ are two sinusoids:

$$F_{11}(t) = K_{11}\sin\Omega_1 t + L_{11}\cos\Omega_1 t \tag{14}$$

$$F_{12}(t) = K_{12}\sin\Omega_2 t + L_{12}\cos\Omega_2 t \tag{15}$$

and:

$$F_2(t) = F_{21}(t) + F_{22}(t) \tag{16}$$

where $F_{21}(t)$ and $F_{22}(t)$ are the two sinusoids:

$$F_{21}(t) = K_{21}\sin\Omega_1 t + L_{21}\cos\Omega_1 t \tag{17}$$

$$F_{22}(t) = K_{22}\sin\Omega_2 t + L_{22}\cos\Omega_2 t \tag{18}$$

The amplitudes K_{ij} and L_{ij} are independent of t. They depend in quite a complex manner on the frequencies Ω_1 and Ω_2 and amplitudes C_1, D_1, C_2, and D_2 of the input signal f(t), plus the frequencies ω_1 and ω_2 of our observer. To find this dependence one can substitute from Eqs. (13-18) into Eqs. (11-12) and determine K_{ij}, L_{ij} by equating the coefficients of terms in $\sin\Omega_1 t$, $\cos\Omega_1 t$, $\sin\Omega_2 t$, and $\cos\Omega_2 t$. This step is very tedious and time consuming and won't be given here explicitly.

2.3 Perfect reconstruction of the input

When our observer operates at the "correct" frequencies, that is, when $\omega_1=\Omega_1$ and $\omega_2=\Omega_2$, then, one can show that the cross-coupling sinusoids $F_{12}(t)$ and $F_{21}(t)$ are identically zero, while $F_1(t)=F_{11}(t)=f_1(t)$, and $F_2(t)=F_{22}(t)=f_2(t)$. In this case $f_1(t)$ is perfectly reproduced by $F_1(t)$, $f_2(t)$ is perfectly reproduced by $F_2(t)$, and the input signal f(t) is perfectly reproduced by the observer signal F(t). Thus, in order to find the amplitudes, phase shifts, and frequencies of the input signal f(t), all we have to do is determine first, in some way, the frequencies Ω_1 and Ω_2. After that, we can simply update the frequencies of our observer to Ω_1 and Ω_2. Then, the signals $F_1(t)$ and $F_2(t)$ produced by our observer will be the same as the sinusoids $f_1(t)$ and $f_2(t)$ respectively.

2.4 Determining the correct frequencies

The reason that the determination of Ω_1 and Ω_2 is not straightforward is that our observer supplies us only with the signals $F_1(t)$ and $F_2(t)$. That is, we have no knowledge of the components $F_{11}(t)$, $F_{12}(t)$,

$F_{21}(t)$, and $F_{22}(t)$ individually. Similarly, we have no knowledge of the components $f_1(t)$ and $f_2(t)$ of f(t) individually. All we know is their sum f(t). Keeping this in mind, the frequencies Ω_1 and Ω_2 can be found by extending the method applied previously to a one-mode signal f(t) in the following way: First, one can examine the explicit expressions for the amplitudes Kij and Lij (not given here) and show that the time derivatives of the functions $F_{ij}(t)$ can be written as:

$$\dot{F}_{11}(t) = \frac{\omega_1 \Omega_1^2}{\pi\left(\Omega_1^2 - \omega_1^2\right)} \left[f_1(t) - F_{21}(t) - f_1(t-T_1) + F_{21}(t-T_1)\right] \tag{19}$$

$$\dot{F}_{12}(t) = \frac{\omega_1 \Omega_2^2}{\pi\left(\Omega_2^2 - \omega_1^2\right)} \left[f_2(t) - F_{22}(t) - f_2(t-T_1) + F_{22}(t-T_1)\right] \tag{20}$$

$$\dot{F}_{21}(t) = \frac{\omega_2 \Omega_1^2}{\pi\left(\Omega_1^2 - \omega_2^2\right)} \left[f_1(t) - F_{11}(t) - f_1(t-T_2) + F_{11}(t-T_2)\right] \tag{21}$$

$$\dot{F}_{22}(t) = \frac{\omega_2 \Omega_2^2}{\pi\left(\Omega_2^2 - \omega_2^2\right)} \left[f_2(t) - F_{12}(t) - f_2(t-T_2) + F_{12}(t-T_2)\right] \tag{22}$$

Then, combining Eqs. (19-20), and using Eqs. (1), (16) one obtains:

$$\left(\frac{\Omega_1^2 - \omega_1^2}{\Omega_1^2}\right)\dot{F}_{11}(t) + \left(\frac{\Omega_2^2 - \omega_1^2}{\Omega_2^2}\right)\dot{F}_{12}(t) = \frac{\omega_1}{\pi}\left[f(t) - F_2(t) - f(t-T_1) + F_2(t-T_1)\right] \tag{23}$$

Similarly, combining Eqs. (21-22), and using Eqs. (1), (13) results in:

$$\left(\frac{\Omega_1^2 - \omega_2^2}{\Omega_1^2}\right)\dot{F}_{21}(t) + \left(\frac{\Omega_2^2 - \omega_2^2}{\Omega_2^2}\right)\dot{F}_{22}(t) = \frac{\omega_2}{\pi}\left[f(t) - F_1(t) - f(t-T_2) + F_1(t-T_2)\right] \tag{24}$$

Denoting the terms in the brackets above by $M_1(t)$ and $M_2(t)$:

$$M_1(t) = f(t) - F_2(t) - f(t-T_1) + F_2(t-T_1) \tag{25}$$

$$M_2(t) = f(t) - F_1(t) - f(t-T_2) + F_1(t-T_2) \tag{26}$$

and using Eqs. (13), (16), one can write Eqs. (23), (24) as:

$$\frac{\omega_1^2}{\Omega_1^2}\dot{F}_{11}(t)+\frac{\omega_1^2}{\Omega_2^2}\dot{F}_{12}(t)=\dot{F}_1(t)-\frac{\omega_1}{\pi}M_1(t) \tag{27}$$

$$\frac{\omega_2^2}{\Omega_1^2}\dot{F}_{21}(t)+\frac{\omega_2^2}{\Omega_2^2}\dot{F}_{22}(t)=\dot{F}_2(t)-\frac{\omega_2}{\pi}M_2(t) \tag{28}$$

Defining two auxiliary variables by:

$$N_1(t)=\dot{F}_1(t)-\frac{\omega_1}{\pi}M_1(t)\,,\qquad N_2(t)=\dot{F}_2(t)-\frac{\omega_2}{\pi}M_2(t) \tag{29}$$

and using again Eqs. (13), (16), one can further manipulate Eqs. (27) and (28) into the form:

$$\frac{1}{\Omega_1^2}\dot{F}_1(t)+\left(\frac{1}{\Omega_2^2}-\frac{1}{\Omega_1^2}\right)\dot{F}_{12}(t)=\frac{N_1(t)}{\omega_1^2} \tag{30}$$

$$\left(\frac{1}{\Omega_1^2}-\frac{1}{\Omega_2^2}\right)\dot{F}_{21}(t)+\frac{1}{\Omega_2^2}\dot{F}_2(t)=\frac{N_2(t)}{\omega_2^2} \tag{31}$$

We want to solve Eqs. (30-31) for Ω_1, Ω_2, but the problem is that we don't know the cross-components $F_{12}(t)$, $F_{21}(t)$ (see Eqs. (13-18)). If the observer frequencies ω_1, ω_2 are close enough to the input frequencies Ω_1, Ω_2 respectively, then, by examining the corresponding expressions for the amplitudes K_{ij}, L_{ij}, of $F_{ij}(t)$ (not given here explicitly), one can show that K_{12}, L_{12}, and K_{21}, L_{21}, are much smaller compared to K_{11}, L_{11}, and K_{22}, L_{22}, respectively. In such a case, it is safe to neglect the time derivatives of $F_{12}(t)$, $F_{21}(t)$ in Eqs. (30-31), and solve these equations approximately for Ω_1, Ω_2 as:

$$\Omega_1^2=\frac{\pi\,\omega_1^2\,\dot{F}_1(t)}{\pi\,\dot{F}_1(t)-\omega_1\left[f(t)-F_2(t)-f(t-T_1)+F_2(t-T_1)\right]} \tag{32}$$

$$\Omega_2^2=\frac{\pi\,\omega_2^2\,\dot{F}_2(t)}{\pi\,\dot{F}_2(t)-\omega_2\left[f(t)-F_1(t)-f(t-T_2)+F_1(t-T_2)\right]} \tag{33}$$

2.5 Comparison with the old frequency adaptation scheme

Before proceeding further, it is interesting to see the connection between Eqs. (32-33) and the frequency adaptation used in our present day observer. To make this connection, consider first an input signal f(t) which is a single sinusoid with frequency Ω. If F(t) is the corresponding (single) observer signal that we use to reproduce f(t), and if ω is the frequency of our observer, then Ω can be found from

the old adaptation formula, derived by Dr. Neumeier, who worked with the quantities A(t) and B(t) rather than F(t). Using our notation this old adaptation formula can be written as:

$$\Omega^2 = \frac{\pi\,\omega^2\,\dot{F}(t)}{\pi\,\dot{F}(t) - \omega\,[f(t) - f(t-T)]} \tag{34}$$

Eq. (34) supplies us with the exact value of Ω, as long as f(t) is a single sinusoid. If we now consider an input signal f(t) which is a sum of n sinusoids, the intuitive way to generalize Eq. (34) would be:

$$\Omega_i^2 = \frac{\pi\,\omega_i^2\,\dot{F}_i(t)}{\pi\,\dot{F}_i(t) - \omega_i \left\{ f(t) - f(t-T_i) - \sum_{j=1,\, j\neq i}^{n} \left[F_j(t) - F_j(t-T_i) \right] \right\}} \qquad i = 1,2,\ldots,n \tag{35}$$

Clearly, Eqs. (32-33) correspond to the special case n=2 in Eq. (35). What is done in our present day observer corresponds basically to using Eq. (35) in an iterative scheme to determine the frequencies Ω_i of an input signal. The iterations are needed partly because Eq. (35) is only approximate, since it ignores the coupling terms $F_{ij}(t)$, and partly because real signals may have characteristics that change with time, like component frequencies, amplitudes, phase shifts, etc.

2.6 Accurate frequency adaptation for two modes

We can try to improve this situation by obtaining a more accurate way of determining the component frequencies Ω_i for input signals composed of n sinusoids. We will first do this for the case n=2, then generalize it to an arbitrary n.

For n=2 we have to reconsider the exact Eqs. (30-31). These equations are valid at any instant of time t, in particular, they are valid for the time instants t-Δt, and t+Δt, where Δt can be taken as a known, strictly positive, and apart from that arbitrary time increment. Explicitly, at t-Δt one has:

$$\frac{1}{\Omega_1^2}\dot{F}_1(t-\Delta t) + \left(\frac{1}{\Omega_2^2} - \frac{1}{\Omega_1^2}\right)\dot{F}_{12}(t-\Delta t) = \frac{N_1(t-\Delta t)}{\omega_1^2} \tag{36}$$

$$\left(\frac{1}{\Omega_1^2} - \frac{1}{\Omega_2^2}\right)\dot{F}_{21}(t-\Delta t) + \frac{1}{\Omega_2^2}\dot{F}_2(t-\Delta t) = \frac{N_2(t-\Delta t)}{\omega_2^2} \tag{37}$$

and, at t+Δt one similarly has:

$$\frac{1}{\Omega_1^2}\dot{F}_1(t+\Delta t)+\left(\frac{1}{\Omega_2^2}-\frac{1}{\Omega_1^2}\right)\dot{F}_{12}(t+\Delta t) = \frac{N_1(t+\Delta t)}{\omega_1^2} \tag{38}$$

$$\left(\frac{1}{\Omega_1^2}-\frac{1}{\Omega_2^2}\right)\dot{F}_{21}(t+\Delta t)+\frac{1}{\Omega_2^2}\dot{F}_2(t+\Delta t) = \frac{N_2(t+\Delta t)}{\omega_2^2} \tag{39}$$

From Eqs. (15), one can now show that:

$$\dot{F}_{12}(t-\Delta t) = \dot{F}_{12}(t)\cos(\Omega_2\Delta t) + \Omega_2 F_{12}(t)\sin(\Omega_2\Delta t) \tag{40}$$

$$\dot{F}_{12}(t+\Delta t) = \dot{F}_{12}(t)\cos(\Omega_2\Delta t) - \Omega_2 F_{12}(t)\sin(\Omega_2\Delta t) \tag{41}$$

Similarly, from Eqs. (17), one can show that:

$$\dot{F}_{21}(t-\Delta t) = \dot{F}_{21}(t)\cos(\Omega_1\Delta t) + \Omega_1 F_{21}(t)\sin(\Omega_1\Delta t) \tag{42}$$

$$\dot{F}_{21}(t+\Delta t) = \dot{F}_{21}(t)\cos(\Omega_1\Delta t) - \Omega_1 F_{21}(t)\sin(\Omega_1\Delta t) \tag{43}$$

Substituting back from Eqs. (40-43) into Eqs. (36-39) we get:

$$\frac{1}{\Omega_1^2}\dot{F}_1(t-\Delta t)+\left(\frac{1}{\Omega_2^2}-\frac{1}{\Omega_1^2}\right)\left[\dot{F}_{12}(t)\cos(\Omega_2\Delta t) + \Omega_2 F_{12}(t)\sin(\Omega_2\Delta t)\right] = \frac{N_1(t-\Delta t)}{\omega_1^2} \tag{44}$$

$$\left(\frac{1}{\Omega_1^2}-\frac{1}{\Omega_2^2}\right)\left[\dot{F}_{21}(t)\cos(\Omega_1\Delta t) + \Omega_1 F_{21}(t)\sin(\Omega_1\Delta t)\right]+\frac{1}{\Omega_2^2}\dot{F}_2(t-\Delta t) = \frac{N_2(t-\Delta t)}{\omega_2^2} \tag{45}$$

$$\frac{1}{\Omega_1^2}\dot{F}_1(t+\Delta t)+\left(\frac{1}{\Omega_2^2}-\frac{1}{\Omega_1^2}\right)\left[\dot{F}_{12}(t)\cos(\Omega_2\Delta t) - \Omega_2 F_{12}(t)\sin(\Omega_2\Delta t)\right] = \frac{N_1(t+\Delta t)}{\omega_1^2} \tag{46}$$

$$\left(\frac{1}{\Omega_1^2}-\frac{1}{\Omega_2^2}\right)\left[\dot{F}_{21}(t)\cos(\Omega_1\Delta t) - \Omega_1 F_{21}(t)\sin(\Omega_1\Delta t)\right]+\frac{1}{\Omega_2^2}\dot{F}_2(t+\Delta t) = \frac{N_2(t+\Delta t)}{\omega_2^2} \tag{47}$$

Equations (44-47), together with Eqs. (30-31) constitute a set of six equations in six unknowns. The unknowns are the four quantities Ω_1, Ω_2, $F_{12}(t)$, $F_{21}(t)$, and the time derivatives of $F_{12}(t)$ and $F_{21}(t)$. From Eqs. (30), (44), and (46), eliminating $F_{12}(t)$ and its time derivative one obtains:

$$\Omega_1^2 = \omega_1^2\left[\frac{2\dot{F}_1(t)\cos(\Omega_2\Delta t) - \dot{F}_1(t+\Delta t) - \dot{F}_1(t-\Delta t)}{2N_1(t)\cos(\Omega_2\Delta t) - N_1(t+\Delta t) - N_1(t-\Delta t)}\right] \tag{48}$$

Similarly, from Eqs. (31), (45), and (47), eliminating $F_{21}(t)$ and its time derivative results in:

$$\Omega_2^2 = \omega_2^2\left[\frac{2\dot{F}_2(t)\cos(\Omega_1\Delta t) - \dot{F}_2(t+\Delta t) - \dot{F}_2(t-\Delta t)}{2N_2(t)\cos(\Omega_1\Delta t) - N_2(t+\Delta t) - N_2(t-\Delta t)}\right] \tag{49}$$

Equations (48-49) must now be solved for the two unknown frequencies Ω_1 and Ω_2. In general, this requires the application of a numerical iterative scheme. If we select a very small time increment Δt, say, equal to the integration time step for the observer signals $F_1(t)$ and $F_2(t)$, then, we can presumably approximate the cosines in Eqs. (48-49) as:

$$\cos(\Omega_1\Delta t) \approx 1 - \frac{\Omega_1^2\Delta t^2}{2}, \qquad \cos(\Omega_2\Delta t) \approx 1 - \frac{\Omega_2^2\Delta t^2}{2} \tag{50}$$

In this case Eqs. (48-49) can be solved analytically. If Δt is small enough so that the cosines can be approximated by unity, then, Eqs. (48-49) decouple and supply us with the solution:

$$\Omega_1^2 = \omega_1^2\left[\frac{2\dot{F}_1(t) - \dot{F}_1(t+\Delta t) - \dot{F}_1(t-\Delta t)}{2N_1(t) - N_1(t+\Delta t) - N_1(t-\Delta t)}\right], \qquad \text{as } \Delta t \to 0 \tag{51}$$

$$\Omega_2^2 = \omega_2^2\left[\frac{2\dot{F}_2(t) - \dot{F}_2(t+\Delta t) - \dot{F}_2(t-\Delta t)}{2N_2(t) - N_2(t+\Delta t) - N_2(t-\Delta t)}\right], \qquad \text{as } \Delta t \to 0 \tag{52}$$

for the frequencies Ω_1 and Ω_2. This solution tends to the exact solution as Δt tends to zero. In practice, for a finite, small Δt the solution expressed in Eqs. (51-52) is either close enough to the exact solution, or if not, it can be used as a first guess for the iterative solution (at a fixed t) of Eqs. (48-49).

3. Extending the Theory of the Observer to n modes

3.1 The input signal

With the two-mode case in the background, the general case of n modes now becomes more transparent. Consider again a signal f(t) given by:

$$f(t) = \sum_{i=1}^{n} f_i(t) \tag{53}$$

where $f_i(t)$ are individual sinusoids:

$$f_i(t) = C_i \sin\Omega_i t + D_i \cos\Omega_i t\,, \qquad i = 1,2,....,n \tag{54}$$

Assume again that:

(i) We know f(t) at each instant of time t.

(ii) We know that f(t) is a sum of n sinusoids, where, n is known.

Again, based on the information given in (i), (ii), we would like to determine the frequencies Ω_i, and the amplitudes C_i, D_i of f(t).

3.2 The observer

To solve the problem, we set up again an observer signal F(t) which is equal to the sum:

$$F(t) = \sum_{i=1}^{n} F_i(t) \tag{55}$$

where, in analogy with Eqs. (11-12), $F_i(t)$ are given by:

$$F_i(t) = \frac{2}{T_i} \int_{t-T_i}^{t} \left[f(\tau) - \sum_{j=1,\, j\neq i}^{n} F_j(\tau) \right] \cos\omega_i(t-\tau)\, d\tau\,, \qquad i = 1,2,....,n \tag{56}$$

For the particular f(t) given by Eqs. (53-54), the solution of Eqs. (56) can be expressed as:

$$F_i(t) = \sum_{j=1}^{n} F_{ij}(t)\,, \qquad i = 1,2,.....,n \tag{57}$$

where $F_{ij}(t)$ are individual sinusoids:

$$F_{ij}(t) = K_{ij} \sin\Omega_j t + L_{ij} \cos\Omega_j t\,, \qquad i = 1,2,..,n, \qquad j = 1,2,..,n \tag{58}$$

The amplitudes K_{ij} and L_{ij} are independent of t. As in the two-mode case, they depend on the frequencies Ω_i and amplitudes C_i, D_i, of the input signal f(t), plus the frequencies ω_i of the observer. To guess this dependence one substitutes from Eqs. (57-58) into Eqs. (56) and determines K_{ij}, L_{ij} by equating the coefficients of terms in $\sin\Omega_i t$ and $\cos\Omega_i t$.

3.3 Perfect reconstruction of the input

In analogy with the two-mode case, one can show that an observer operating at the frequencies $\omega_i = \Omega_i$ reproduces the input signal perfectly. In this case all the cross-coupling sinusoids $F_{ij}(t)$, $i \neq j$, are identically zero, while $F_{ii}(t) = f_i(t)$. Thus, to find the characteristics of the input signal, we must again first determine the input frequencies Ω_i.

3.4 Determining the correct frequencies

Before determining the frequencies Ω_i we have to note that we know only f(t) and the signals $F_i(t)$ supplied to us by our observer. We have no knowledge of the individual components $F_{ij}(t)$ of the observer, or the individual components $f_i(t)$ of the input. Luckily, Eqs. (19-22) which led to the determination of Ω_i in the two-mode case afford a straightforward generalization for the present case. By examining the explicit expressions for the amplitudes Kij and Lij (not given here) one can show that the time derivatives of the functions $F_{ij}(t)$ can be written as:

$$\dot{F}_{ij}(t) = \frac{\omega_i \Omega_j^2}{\pi\left(\Omega_j^2 - \omega_i^2\right)} \left\{ f_j(t) - f_j(t - T_i) - \sum_{k=1,k\neq i}^{n} \left[F_{kj}(t) - F_{kj}(t - T_i) \right] \right\} \tag{59}$$

Rearranging the above expression and summing over the index j one obtains:

$$\sum_{j=1}^{n} \left(\frac{\Omega_j^2 - \omega_i^2}{\Omega_j^2} \right) \dot{F}_{ij}(t) = \frac{\omega_i}{\pi} \left\{ \sum_{j=1}^{n} \left[f_j(t) - f_j(t - T_i) \right] - \sum_{j=1}^{n} \sum_{k=1,k\neq i}^{n} \left[F_{kj}(t) - F_{kj}(t - T_i) \right] \right\} \tag{60}$$

The sum on the left-hand-side can be simplified by using Eq. (57). The first sum on the right-hand-side can be simplified by using Eq. (53). For the double sum on the right-hand-side one first uses Eq. (57) and sums with respect to j, then the dummy index k is changed to j. After rearranging terms, Eq. (60) can be written in the equivalent form:

$$\sum_{j=1}^{n} \left(\frac{\omega_i^2}{\Omega_j^2} \right) \dot{F}_{ij}(t) = \dot{F}_i(t) - \frac{\omega_i}{\pi} \left\{ f(t) - f(t - T_i) - \sum_{j=1,j\neq i}^{n} \left[F_j(t) - F_j(t - T_i) \right] \right\} \tag{61}$$

Just as in Eqs. (25-26), defining the auxiliary quantities $M_i(t)$ by:

$$M_i(t) = f(t) - f(t - T_i) - \sum_{j=1,j\neq i}^{n} \left[F_j(t) - F_j(t - T_i) \right], \qquad i = 1,2,\ldots..,n \tag{62}$$

one can write Eq. (61) as (see Eqs. (27-28)):

$$\sum_{j=1}^{n} \left(\frac{\omega_i^2}{\Omega_j^2} \right) \dot{F}_{ij}(t) = \dot{F}_i(t) - \frac{\omega_i}{\pi} M_i(t) \tag{63}$$

Then, using the definitions (see Eqs. (29)):

$$N_i(t) = \dot{F}_i(t) - \frac{\omega_i}{\pi} M_i(t), \qquad i = 1,2,.....,n \tag{64}$$

and Eq. (57), one can write Eq. (64) in a form completely analogous to Eqs. (30-31):

$$\frac{1}{\Omega_i^2}\dot{F}_i(t) + \sum_{j=1,\, j\neq i}^{n}\left(\frac{1}{\Omega_j^2} - \frac{1}{\Omega_i^2}\right)\dot{F}_{ij}(t) = \frac{N_i(t)}{\omega_i^2}, \qquad i = 1,2,.....,n \tag{65}$$

To solve the above n equations for Ω_i we first need to have sufficient information to determine the cross-coupling sinusoids $F_{ij}(t)$. Extending the procedure followed in section 2.6, we can select an integer m, and write equations identical to Eqs. (65), valid at the 2m instants of time t-kΔt, t+kΔt, with k=1,2,....,m. We thus obtain an additional 2mn equations (just like Eqs. (36-39) in the two-mode case). In each one of these equations, just as in Eqs. (40-42), we use the identities:

$$\dot{F}_{ij}(t - k\Delta t) = \dot{F}_{ij}(t)\cos\left(k\Omega_j\Delta t\right) + \Omega_j F_{ij}(t)\sin\left(k\Omega_j\Delta t\right) \tag{66}$$

$$\dot{F}_{ij}(t + k\Delta t) = \dot{F}_{ij}(t)\cos\left(k\Omega_j\Delta t\right) - \Omega_j F_{ij}(t)\sin\left(k\Omega_j\Delta t\right) \tag{67}$$

Then, we have a total of $2n^2$-n unknowns. The unknowns are the n frequencies Ω_i, the n^2-n quantities $F_{ij}(t)$, and the n^2-n derivatives of $F_{ij}(t)$. We also have 2mn+n equations, n of them given by Eqs. (65), and 2mn of them given by (see Eqs. (44-47)):

$$\frac{1}{\Omega_i^2}\dot{F}_i(t - k\Delta t) + \sum_{j=1,\, j\neq i}^{n}\left(\frac{1}{\Omega_j^2} - \frac{1}{\Omega_i^2}\right)\left[\dot{F}_{ij}(t)\cos\left(k\Omega_j\Delta t\right) + \Omega_j F_{ij}(t)\sin\left(k\Omega_j\Delta t\right)\right] = \frac{N_i(t - k\Delta t)}{\omega_i^2} \tag{68}$$

$$\frac{1}{\Omega_i^2}\dot{F}_i(t + k\Delta t) + \sum_{j=1,\, j\neq i}^{n}\left(\frac{1}{\Omega_j^2} - \frac{1}{\Omega_i^2}\right)\left[\dot{F}_{ij}(t)\cos\left(k\Omega_j\Delta t\right) - \Omega_j F_{ij}(t)\sin\left(k\Omega_j\Delta t\right)\right] = \frac{N_i(t + k\Delta t)}{\omega_i^2} \tag{69}$$

Sufficient information for a solution is thus provided when 2mn+n=$2n^2$-n. This determines the value of m as m=n-1. Adding Eqs. (68-69) one obtains:

$$\sum_{j=1,\, j\neq i}^{n}\left(\frac{1}{\Omega_j^2} - \frac{1}{\Omega_i^2}\right)\dot{F}_{ij}(t)\cos\left(k\Omega_j\Delta t\right) = \frac{N_i(t + k\Delta t) + N_i(t - k\Delta t)}{2\omega_i^2} - \frac{\dot{F}_i(t + k\Delta t) + \dot{F}_i(t - k\Delta t)}{2\Omega_i^2} \tag{70}$$

For m=n-1, Eqs. (70) constitute a set of $mn=n^2-n$ equations that can be used to eliminate the n^2-n time derivatives of $F_{ij}(t)$. The resulting expressions for these time derivatives can then be substituted into Eqs. (65), supplying us with a system of n equations in the n frequencies Ω_i. Just as in the two-mode case, a complete solution for the frequencies Ω_i can be obtained when the time increment Δt tends to zero. In this case all the cosines can be safely replaced by unity, and Eq. (70) becomes:

$$\sum_{j=1,\, j\neq i}^{n}\left(\frac{1}{\Omega_j^2}-\frac{1}{\Omega_i^2}\right)\dot{F}_{ij}(t) = \frac{N_i(t+k\Delta t)+N_i(t-k\Delta t)}{2\omega_i^2} - \frac{\dot{F}_i(t+k\Delta t)+\dot{F}_i(t-k\Delta t)}{2\Omega_i^2}, \quad \text{as } \Delta t\to 0 \qquad (71)$$

Substituting from Eq. (71) into Eq. (65), and taking k=1, results in a set of n decoupled equations which can be solved for the frequencies Ω_i as:

$$\Omega_i^2 = \omega_i^2\left[\frac{2\dot{F}_i(t)-\dot{F}_i(t+\Delta t)-\dot{F}_i(t-\Delta t)}{2N_i(t)-N_i(t+\Delta t)-N_i(t-\Delta t)}\right], \quad \text{as } \Delta t\to 0, \quad i=1,2,.....,n \qquad (72)$$

This solution is qualitatively identical to the one obtained for the two-mode case (compare with Eqs. (51-52)), and tends to the exact solution for Ω_i as Δt tends to zero. In practice, for a finite, small Δt the solution expressed in Eqs. (72) is either close enough to the exact solution, or if not, it can be used as a first guess for the iterative solution (at a fixed t) of Eqs. (65), (70).

Appendix B

High Frequency Nonlinear Vibrational Control

B. Shapiro and B. T. Zinn

Submitted for publication to the IEEE Transaction on Automatic Control.

HIGH FREQUENCY NONLINEAR VIBRATIONAL CONTROL

B. Shapiro* and B. T. Zinn†

Abstract

This paper discusses the feasibility of high frequency nonlinear vibrational control. Such control has the advantage that it does not require state measurement and processing capabilities that are required in conventional feedback control. Bellman, Bentsman, and Meerkov (1986) investigated nonlinear systems controlled by linear vibrational controllers and proved that vibrational control is not feasible if the Jacobian matrix has a positive trace. This paper extends previous work to include nonlinear vibrational controllers. A stability criteria is derived for nonlinear systems with nonlinear controllers, and it is shown that a nonlinear vibrational controller can stabilize a system even if the Jacobian matrix has a positive trace.

Preferred Address

B. Shapiro, P.O. 38176, Georgia Tech Station, Atlanta GA, 30332, (before September 3rd).

B. Shapiro, Control and Dynamical Systems, Mail Code 104-44, California Institute of Technology, Pasadena, CA 91125, (after September 3rd).

Acknowledgment

This work benefited from many helpful discussions with Dr. J. Hale; and was supported by funds provided by the Davis S. Lewis Jr. Chair and AFOSR contract number F49620-93-1-0177, Dr. Mitar Birkan, contract monitor.

*School of Aerospace Engineering, Georgia Institute of Technology, Atlanta, GA 30332. Email: gt8176b@prism.gatech.edu Tel: (404) 325-4714.

†School of Aerospace Engineering, Georgia Institute of Technology, Atlanta, GA 30332. Email: ben.zinn@aerospace.gatech.edu Tel: (404) 894-3033

1 Introduction

This paper discusses the feasibility of applying open loop control in the form of high frequency vibrational control to engineering systems. Such control may be applied in cases where closed loop control is impractical and has the advantage that it does not require costly sensing and computing capabilities. Vibrational control is applied by oscillating an accessible system component at low amplitude and high frequency (relative to the natural frequency of the system). For example, an inverted pendulum can be stabilized by vertically oscillating the pendulum pin at a sufficiently high frequency and low amplitude. Let us examine the case of the pendulum in more detail. The vertically oscillated pendulum is described by the following nonlinear differential equation,

$$\dot{x}_1 = x_2, \tag{1.1}$$

$$\dot{x}_2 = C\sin(x_1) - Bx_2 + aw^2 D\sin(x_1)\sin(wt), \tag{1.2}$$

where x_1 is the angular displacement measured from the inverted equilibrium point, x_2 is the angular velocity, B, C and D are positive physical constants, and a and w are the amplitude and frequency of the applied vibration, respectively. In this example, the control input is the applied vibration, which is given by $a\sin(wt)$. Note that the amplitude and frequency of the control input are constant and, therefore, independent of the state of the system. Since there is no sensing or computation involved, this is a form of open loop control. However, (1.2) involves a feedback-like term $w^2 D\sin(x_1)$, which occurs naturally as a result of the moment arm $\sin(x_1)$ between the vertically oscillating pendulum pin and the center of mass of the pendulum. Consequently, the feedback $w^2 D\sin(x_1)$ is *naturally occurring*.

Vertically vibrated pendulum

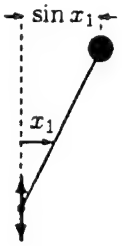

Horizontally vibrated pendulum

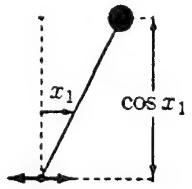

Since the naturally occurring feedback $w^2 D\sin(x_1)$ in (1.2) is of the same form as $C\sin(x_1)$, we can view this form of control as a variation of the parameter C; that is,

$$\dot{x}_1 = x_2, \tag{1.3}$$

$$\dot{x}_2 = [C + aw^2 D\sin(wt)]\sin(x_1) - Bx_2. \tag{1.4}$$

Linearization of the above system yields

$$\begin{bmatrix} \dot{x}_1 \\ \dot{x}_2 \end{bmatrix} = \begin{bmatrix} 0 & 1 \\ C + aw^2 D\sin(wt) & -B \end{bmatrix} \begin{bmatrix} x_1 \\ x_2 \end{bmatrix}, \tag{1.5}$$

which is of the form

$$\dot{x} = [\mathcal{A} + \mathcal{B}(t)]x, \tag{1.6}$$

where x is a vector, $\mathcal{A}$ is a constant matrix and $\mathcal{B}(t)$ is a time-varying matrix. In the linear model (1.6), vibrational control appears as a variation of parameters, where the parameters of the matrix $\mathcal{A}$ are varied by $\mathcal{B}(t)$. This is the model investigated by Bellman, Bentsman and Meerkov [1]. However, there is no reason to assume that vibrational control can always be viewed as a variation of parameters as in the above example. In fact, there are examples where the above model does not apply.

Consider the pendulum once again. Suppose we oscillate the pin of the pendulum horizontally instead of vertically, producing motions that are described by

$$\dot{x}_1 = x_2, \tag{1.7}$$

$$\dot{x}_2 = C\sin(x_1) - Bx_2 + aw^2 D\cos(x_1)\sin(wt). \tag{1.8}$$

Instead of the moment arm $\sin(x_1)$ we now have a moment arm $\cos(x_1)$ and the naturally occurring feedback is $w^2 D\cos(x_1)$. Linearization of this system of equations yields

$$\begin{bmatrix} \dot{x}_1 \\ \dot{x}_2 \end{bmatrix} = \begin{bmatrix} 0 & 1 \\ C & -B \end{bmatrix} \begin{bmatrix} x_1 \\ x_2 \end{bmatrix} + \begin{bmatrix} 0 \\ aw^2 D\sin(wt) \end{bmatrix}, \tag{1.9}$$

which cannot be written in the form of (1.6). Consequently, we cannot view the above case as a variation of parameters.

The above example demonstrates that vibrating a system component does not always produce "variation of parameters" as in the vertically vibrated pendulum. Consequently, we adopt a more general approach that permits the analysis of problems where a vibrated system component may result in nonlinear functions in the governing equations. Consider a nonlinear system

$$\dot{x} = f(x), \tag{1.10}$$

with an equilibrium point at the origin (i.e., $f(0) = 0$). Vibrational control is applied by oscillating a system component or process at high frequency and low amplitude. For instance, in the case of a jet engine, the air-throttle or amount of fuel injected might be vibrated. Let $h(wt) = \sin(wt)$ denote the applied high frequency vibration. It is assumed that the vibration affects the system $f(x)$ through some naturally occurring feedback function $g(x, w, a)$, which depends on the vibrated component. The vibrationally controlled system is described by

$$\dot{x} = f(x) + h(wt)g(x, w, a). \tag{1.11}$$

For convenience, the amplitude of $h(wt)$ is taken to equal unity and the amplitude of the applied vibration is accounted for by $g(x, w, a)$. In the case of the pendulum,

$$f(x) = [x_2, C\sin(x_1) - Bx_2]^T \tag{1.12}$$

and $g(x, w, a) = [0, aw^2 D\sin(x_1)]^T$ for the vertically vibrated pin, or $g(x, w, a) = [0, aw^2 D\cos(x_1)]^T$ for the horizontally vibrated pin. We emphasize once again that $g(x, w, a)$ occurs naturally, and is not measured or computed but is a result of the interaction between the system and vibrated component. Obviously, an oscillating fuel injection rate is not going to affect the jet engine in the same fashion as an oscillating throttle. Consequently, each actuation will be described by a different function $g(x, w, a)$. Since $g(x, w, a)$ depends on properties of the system (which are fixed) and the vibrated component, we can only control the choice of the component to oscillate and the frequency and amplitude of the vibration. This choice determines the form of $g(x, w, a)$, and since in certain cases there exist no $g(x, w, a)$ that will allow vibrational control, such control is not always feasible.

We now turn to the question of stability. Suppose the equilibrium point $x = 0$ of (1.10) is unstable, and that there exist one or more accessible system components or processes that can be vibrated, each associated with a function $g(x, w, a)$ that is known. The objective of the theory presented in this paper is to determine a stability criterion for (1.11). Consequently, if a certain $g(x, w, a)$ satisfies the derived stability criterion, then oscillation of the corresponding system component, with specific frequency w and amplitude a, will alter the stability of the system and result in vibrational control. Therefore, the developed criterion will determine if vibrational control is feasible for various accessible system components or processes in a given system.

Vibrational control has found various applications, including lasers [2] and particle beams [3]. Initial work on developing a general theory of vibrational control was carried out by Meerkov [4]. He discussed the effect of vibrational control upon stability, transient motion and response of the controlled system. In subsequent publications, several specific nonlinear problems were discussed [5], but no general vibrational control was proposed. Such a theory was outlined by Bellman, Bentsman and Meerkov [1], who presented criteria for the control of nonlinear systems by linear vibrational control. Further nonlinear results are discussed in [6], including conditions for and choice of stabilizing vibrations.

To discuss the results derived in [1], consider (1.11) and assume that the Jacobian matrix $\partial f(0)/\partial x = f'(0)$ of $f(x)$ in (1.11) has a positive trace. A classic theorem in linear algebra states that the trace of a matrix equals the sum of its eigenvalues (see for example [7, p.251]). Consequently, if the trace is positive, then at least one of the

eigenvalues must have a positive real part and the equilibrium point is unstable. This does not imply, however, that if the trace is negative the equilibrium point is stable. A negative trace is a necessary but not a sufficient condition for stability.

Bellman, Bentsman and Meerkov [1] only considered linear vibrational control, which limited the analysis to linear functions $g(x,a,w) = Mx$ in (1.11). They proved that if the Jacobian $f'(0)$ has a positive trace and $g(x,a,w)$ is linear, then vibrational control is not feasible, indicating that no matrix M can stabilize the system (1.11). In this paper we consider a more general case of vibrational control via a nonlinear, slowly varying $g(x,a,w)$. In other words, we consider functions whose rate of change with respect to x is bounded (i.e., $\|\partial g/\partial x\| \leq w\delta_1$). We show that in this case, vibrational control may be possible even if the trace of the Jacobian Matrix is positive. Specifically, it will be shown that there exist nonlinear functions $g(x,a,w)$ that stabilize the system (1.11) even if its Jacobian $f'(0)$ has a positive trace.

The main point of this paper is that nonlinearities in $g(x,a,w)$ may not be negligible, and can affect the stability of (1.11). This result is of practical importance for the following reason. In engineering, it is common practice to linearize a system before analyzing its stability. However, if a linear system is considered, then Bellman, Bentsman and Meerkov's result indicates that vibrational control is not feasible when the Jacobian has a positive trace (note that positive traces occur in a wide variety of engineering systems e.g., liquid rockets [8]). Most engineering systems are, however, nonlinear and it is possible that nonlinearities in $g(x,a,w)$ may stabilize the system even if its Jacobian trace is positive. This implies that one should not discount vibrational control for systems that exhibit a positive trace. Instead, one should investigate the nonlinear functions $g(x,a,w)$ associated with vibrational open loop control to determine if they satisfy the stability criteria derived in this paper. We also note that the theory presented in this paper agrees almost exactly with numerical solutions (see section. 3.1).

2 General Derivation

Consider once again the nonlinear system

$$\dot{x} = f(x) + h(wt)g(x,w,a), \tag{2.1}$$

where $h(wt) = \sin(wt)$, $x \in \mathbb{R}^n$ is the state space vector and $x = 0$ is an equilibrium point of (1.10), which is not necessarily an equilibrium point of the forced system (2.1). It is assumed that $f(x)$ is three times continuously differentiable and $g(x)$ is four times continuously differentiable.

We will show that the nonautonomous system (2.1) can be approximated by an autonomous system

$$\dot{y} = F(y). \tag{2.2}$$

This approximation means that there exists a function $u(t,y)$, which is small for all time, such that $x(t) = y(t)+u(t,y)$. Consequently, if $Y(t)$ is a solution of (2.2) and $X(t)$ is a solution of (2.1), then $X(t)-Y(t) = u(t,Y(t))$ is small for all time t. Approximately, $Y(t)$ corresponds to the time average of $X(t)$, and it describes the slow response of the system, while $u(t,Y(t))$ corresponds to the small amplitude high frequency system oscillations excited by the small amplitude, high frequency control input. In essence, there exist two time scales. A fast time scale corresponding to the high frequency control input and the resulting high frequency system response $u(t,Y(t))$, and the slow time scale describing the time averaged system response $Y(t)$. Since $Y(t)$ is a slow or averaged response, it is described by a time averaged equation. In the case of vibrational control, the control input coupled with the system response $u(t,Y(t))$ yields a non-zero average that can stabilize the system.

We will use the following notation. Since w and a are constant, we will express $g(x,w,a)$ as $g(x)$. Also, we define the Jacobian matrix $J = f'(0) = \partial f(0)/\partial x$ and let

$$p(x) = f(x) - Jx, \tag{2.3}$$

$$\phi(wt) = -\varepsilon^2 Jg(0)\sin(wt) - \varepsilon g(0)\cos(wt), \tag{2.4}$$

where $\varepsilon = 1/w$, and $p(x)$ is the sum of all terms of second order and higher in the Taylor expansion of $f(x)$

around $x = 0$. Furthermore, we introduce the constant vector b

$$b = \left[\frac{1}{T} \int_0^T p(\phi(wt))dt - \frac{\varepsilon^2 g'(0) J g(0)}{2} \right], \tag{2.5}$$

where $T = 2\pi/w$ and $g'(0)$ is the Jacobian matrix of $g(x)$, and the constant matrix A,

$$A = \left[J - \frac{\varepsilon^2}{2} \frac{\partial (g'(y) J g(y))}{\partial y}(0) \right], \tag{2.6}$$

where $g'(y)$ is the derivative of $g(y)$ evaluated at y, and $\partial[g'(y)Jg(y)](0)/\partial y$ denotes the derivative of $g'(y)Jg(y)$ evaluated at zero. Finally, we let

$$\zeta = \delta^2 + \varepsilon^2 \delta_0 \delta_1 + \delta \delta_1^2 + \delta_0 \delta_1^3/\varepsilon + \delta \delta_1^4/\varepsilon + \delta_0^3 + \delta_0^2 \delta_1 + \delta \delta_0^2 + \delta \delta_0 \delta_1 + \varepsilon^3 \delta_0^2 \tag{2.7}$$

and denote a ball of radius δ centered at a as $B(a, \delta)$.

Theorem 2.1 *Consider the nonlinear system (2.1) and suppose that $f(0) = 0$, $\|g(0)\| \leq w\delta_0$, and $\|g'(\xi)\| \leq w\delta_1$ for all $\xi \in B(0, \delta)$. Then for sufficiently small δ, δ_0 and δ_1, and sufficiently large w, there exists a function $u(t, y)$ that satisfies the following properties: $\|u(t, y)\| < 2(\delta_0 + \delta\delta_1)$ for all t and for all $y \in B(0, \delta)$, it is $2\pi/w$ periodic in t, and for any y has zero mean value. Furthermore, for $x(t)$ governed by the differential equation (2.1), $y(t) = x(t) - u(t, y)$ is governed by*

$$\dot{y} = Ay + b + O(\zeta) \tag{2.8}$$

for all $y \in B(0, \delta)$ and b, A and ζ defined in (2.5), (2.6) and (2.7), respectively.

While a detailed proof of Theorem (2.1) is given in the Appendix, an outline of the proof is provided below. A transformation $u(s, y)$ is constructed that satisfies the properties of the theorem. We then substitute the equation $y(t) = x(t) - u(t, y)$ into (2.1) and bound various terms so that we can rewrite (2.1) as the approximate system $\dot{y} = F(t, y)$. Next, we apply the method of averaging to derive the averaged equation $\dot{y} = F_{av}(y)$. Linearization of $\dot{y} = F_{av}(y)$ at the origin yields the result of the theorem.

The analysis in this paper includes Taylor terms up to second order in δ_0 and δ_1. Consequently, the resulting error ζ is of third order. If higher accuracy is desired, then more Taylor terms can be included although more stringent smoothness constraints will be imposed because we will have to ensure that higher order derivatives exist for the functions $f(x)$ and $g(x)$. We note that for the examples considered, a second order analysis is sufficient and is in excellent agreement with numerical integration results (see example 3.1).

2.1 Example: The Inverted Pendulum

Consider the vertically vibrated pendulum described by (1.1) and (1.2). These equations are of the form of (2.1). Since $g(0) = 0$, (2.4) implies that $\phi(wt) = 0$ and (2.3) shows that $p(0) = f(0) - 0 = 0$. Consequently, the vector b defined in (2.5) equals zero. The matrix A is defined in (2.6) and can be expressed in the following form,

$$\begin{aligned} A &= \left[J - \frac{\varepsilon^2}{2} \frac{\partial (g'(y) J g(y))}{\partial y}(0) \right] = J - \frac{\varepsilon^2}{2} \frac{\partial}{\partial y} \left\{ \begin{bmatrix} 0 & 0 \\ aw^2 D \cos(y_1) & 0 \end{bmatrix} \begin{bmatrix} 0 & 1 \\ C & -B \end{bmatrix} \begin{bmatrix} 0 \\ aw^2 D \sin(y_1) \end{bmatrix} \right\} \\ &= \begin{bmatrix} 0 & 1 \\ C & -B \end{bmatrix} - \frac{\partial}{\partial y} \begin{bmatrix} 0 \\ a^2 w^2 D^2 \cos(y_1) \sin(y_1)/2 \end{bmatrix} = \begin{bmatrix} 0 & 1 \\ C - (awD)^2/2 & -B \end{bmatrix}. \end{aligned} \tag{2.9}$$

Consequently, Theorem (2.1) indicates that the averaged behaviour of the system is governed by

$$\begin{bmatrix} \dot{y}_1 \\ \dot{y}_2 \end{bmatrix} = \begin{bmatrix} 0 & 1 \\ C - (awD)^2/2 & -B \end{bmatrix} \begin{bmatrix} y_1 \\ y_2 \end{bmatrix} \tag{2.10}$$

which is in agreement with the result of [4]. Note that the term $C-(awD)^2/2$ is negative for sufficiently large a or w, indicating that the equilibrium point is asymptotically stable. We also note that even though the method in this paper is restricted to slowly varying $g(x)$, (i.e., $\|g'(x)\| \leq w\delta_1 < w$) the above result is also valid for $\|g'(x)\| \not< w$. We impose the slowly varying restriction to permit inverting the matrix $[I+u_y]$ in (5.21). In the case of the pendulum, we can show that the matrix $[I+u_y]$ has an inverse even if $\|g'(x)\| \not< w$, which eliminates the slowly varying restriction.

3 Discussion of Results

Theorem (2.1) implies that vibrational control can result in an equilibrium shift. For such a shift to occur, the vector b defined in (2.5) has to be nonzero. Equations (2.3),(2.4) and (2.5) imply that such an equilibrium shift can occur only if $g(0)$ is nonzero. In this case there are two possibilities. The first possibility is that the average of $p(\phi(wt))$ is nonzero. Since $p(x)$ is defined in (2.3) as the nonlinear terms of $f(x)$, this implies that nonlinearities in $f(x)$ can cause an equilibrium shift. Such an equilibrium shift would be of order $O(\|\phi\|^2) = O(\delta_0^2)$. The second possibility is that the term $g'(0)Jg(0)$ is nonzero, indicating that the naturally occurring feedback function $g(x)$ can also cause an equilibrium shift. In this case, the equilibrium shift would be of order $O(\epsilon^2\|g'(0)Jg(0)\|) = O(\delta_0\delta_1)$. In either case, if the equilibrium shift is larger than δ our analysis fails because we are forced outside the ball $B(0,\delta)$.

Theorem (2.1) also yields a useful linear result. Consider a linear system of the form

$$\dot{x} = [J + \sin(wt)B]x, \tag{3.1}$$

where $\|B\| < w\delta_1$. In this case, $g(x) = Bx$ and $g'(x) = B$. Therefore $g(0) = 0$ and we can set $\delta_0 = 0$ with no loss of generality. Application of Theorem (2.1) yields the averaged equation

$$\dot{y} = [J - \epsilon^2 BJB/2]y + O\left(\delta(\delta + \delta_1^2 + \delta_1^4/\epsilon)\right). \tag{3.2}$$

However, the most interesting implication of Theorem (2.1) is the following: the operator $g'(y)Jg(y)$ in (2.6) is a nonlinear operator in $g(y)$. Consequently, nonlinearities in $g(y)$ may result in linear terms in the averaged equation (2.8), and can influence local stability. This indicates that the local stability of the nonlinear system (1.11) is not the same as the stability of a corresponding linearized system. It is possible to show that the nonlinearities in $g(y)$ can alter the stability of a system with a positive Jacobian trace. Stabilization of a system with a positive trace is illustrated in the next example.

3.1 Example: A System with a Positive Jacobian Trace

In this example we consider a second-order system with a positive trace. Specifically, we consider the second-order system derived in [8] for the flow potential of a liquid rocket combustor,

$$\ddot{x} + A_1\dot{x} + A_0 x = 0, \tag{3.3}$$

where x is a nondimensional flow potential perturbation and t is a normalized time. In an unstable liquid rocket, unsteady combustion provides negative damping that drives the instability. Since the damping is determined by A_1, negative damping corresponds to a negative coefficient A_1. To illustrate the point, we let $A_1 = -0.2$ and $A_0 = 1$, and rewrite (3.3) as the following second order system

$$\begin{bmatrix} \dot{x}_1 \\ \dot{x}_2 \end{bmatrix} = \begin{bmatrix} 0 & 1 \\ -A_0 & -A_1 \end{bmatrix} \begin{bmatrix} x_1 \\ x_2 \end{bmatrix} = \begin{bmatrix} 0 & 1 \\ -1 & 0.2 \end{bmatrix} \begin{bmatrix} x_1 \\ x_2 \end{bmatrix}. \tag{3.4}$$

The Jacobian matrix of (3.4) has a positive trace, indicating that the equilibrium point $x = 0$ is unstable.

Bellman, Bentsman and Meerkov [1] prove that it is not possible to vibrationally control a system with a positive trace if the function $g(x)$ is linear. Consequently, postulate the existence of a nonlinear function $g(x)$

$$g(x) = \begin{bmatrix} 0 \\ \alpha + \beta x_1 x_2 \end{bmatrix} \tag{3.5}$$

that describes the effect produced by forcing a system component. We stress once again that such a $g(x)$ would have to occur naturally. We will now show that if such a nonlinear $g(x)$ exists, it will stabilize the system (we do not claim that such a $g(x)$ is possible in rocket motors). A discussion of the reasoning for choosing the specific nonlinear $g(x)$ given in (3.5) is provided in Section (5.3) in the Appendix.

Given the above choice of $g(x)$, we write the forced equation as

$$\begin{bmatrix} \dot{x}_1 \\ \dot{x}_2 \end{bmatrix} = \begin{bmatrix} 0 & 1 \\ -A_0 & -A_1 \end{bmatrix} \begin{bmatrix} x_1 \\ x_2 \end{bmatrix} + \begin{bmatrix} 0 \\ \alpha + \beta x_1 x_2 \end{bmatrix} \sin(wt). \tag{3.6}$$

Let $w = 70$, $\alpha = 15$ and $\beta = 200$. For these values, (3.6) becomes

$$\begin{bmatrix} \dot{x}_1 \\ \dot{x}_2 \end{bmatrix} = \begin{bmatrix} 0 & 1 \\ -1 & 0.2 \end{bmatrix} \begin{bmatrix} x_1 \\ x_2 \end{bmatrix} + \begin{bmatrix} 0 \\ 15 + 200 x_1 x_2 \end{bmatrix} \sin(wt). \tag{3.7}$$

It follows from (3.5) that $\|g(0)\| \leq \alpha \leq w\delta_0$ for $\delta_0 \approx 0.22$. Similarly $\|g'(x)\| \leq \beta(x_1 + x_2) < 2\beta\delta < w\delta_1$ for $\delta_1 \approx (5.72)\delta$. Consequently, both δ_0 and δ_1 are sufficiently small and we can apply Theorem (2.1).

We need to calculate the vector b and the matrix A defined in (2.5) and (2.6), respectively. Notice that $p(x)$, defined in (2.3), is zero because the system (3.4) is linear. Consequently, (2.5) yields

$$b = -\frac{\varepsilon^2 g'(0) J g(0)}{2}. \tag{3.8}$$

However,

$$g'(x) = \begin{bmatrix} 0 & 0 \\ \beta x_2 & \beta x_1 \end{bmatrix} \tag{3.9}$$

indicating that $g'(0) = 0$, which implies $b = 0$ and that there is no equilibrium shift.

Equation (2.6) yields the matrix A,

$$A = \left[J - \frac{\varepsilon^2}{2} \frac{\partial (g'(y) J g(y))}{\partial y}(0) \right] = J - \frac{\varepsilon^2}{2} \frac{\partial}{\partial y} \left\{ \begin{bmatrix} 0 & 0 \\ \beta y_2 & \beta y_1 \end{bmatrix} \begin{bmatrix} 0 & 1 \\ -A_0 & -A_1 \end{bmatrix} \begin{bmatrix} 0 \\ \alpha + \beta y_1 y_2 \end{bmatrix} \right\}$$

$$= J - \frac{\varepsilon^2}{2} \frac{\partial}{\partial y} \begin{bmatrix} 0 \\ \alpha\beta y_2 - A_1 \alpha\beta y_1 + \beta^2 y_1 y_2^2 - A_1 \beta^2 y_1^2 y_2 \end{bmatrix} = \begin{bmatrix} 0 & 1 \\ -A_0 + \varepsilon^2 A_1 \alpha\beta/2 & -A_1 - \varepsilon^2 \alpha\beta/2 \end{bmatrix}. \tag{3.10}$$

Consequently, Theorem (2.1) implies that the averaged motion of the system is governed by

$$\begin{bmatrix} \dot{y}_1 \\ \dot{y}_2 \end{bmatrix} = \begin{bmatrix} 0 & 1 \\ -A_0 + \varepsilon^2 A_1 \alpha\beta/2 & -A_1 - \varepsilon^2 \alpha\beta/2 \end{bmatrix} \begin{bmatrix} y_1 \\ y_2 \end{bmatrix}. \tag{3.11}$$

Substituting the numerical values for A_0, A_1, α, β and $\varepsilon = 1/w$ yields

$$\begin{bmatrix} \dot{y}_1 \\ \dot{y}_2 \end{bmatrix} = \begin{bmatrix} 0 & 1 \\ -1.061 & -0.106 \end{bmatrix} \begin{bmatrix} y_1 \\ y_2 \end{bmatrix} \tag{3.12}$$

which is asymptotically stable.

Since the solution $X(t)$ of (3.6) is given by $X(t) = Y(t) + u(t, Y(t))$, where $Y(t)$ is a solution of (3.12) and tends towards the origin as time tends to infinity, $X(t)$ must remain close to the origin for all time because $u(t, Y(t))$ is small for all time. The construction of $u(t, y)$, as defined in the Appendix (see (5.4),(5.8) and (5.9)), implies that if $g(0) \neq 0$ then $u(t, y) \not\to 0$ as $y \to 0$. In this case $g(0) \neq 0$, indicating that $u(t, Y(t))$ does not converge to zero as $Y(t)$ tends to zero. Consequently, $X(t)$ remains close to zero for all time but does not tend to zero as time goes to infinity. Strictly speaking, the equilibrium point $x = 0$ of (2.1) is not asymptotically stable; indeed $x = 0$ is not an equilibrium point but is the center of a small asymptotically stable limit cycle. This limit cycle is the asymptotically stable orbit $X(t) = u(t, 0) \neq 0$. We refer to $x = 0$ as a *slow equilibrium point* because $y = 0$ is an equilibrium point of the slow or time averaged system (2.8), and we say that $x = 0$ is

slowly asymptotically stable because the equilibrium point $y = 0$ of the slow system (2.8) is asymptotically stable. When we refer to *slow* equilibrium points or *slow* stability, we refer to the properties of the time averaged system (2.8). The true dynamics are small oscillations about the slow or averaged dynamics and hence display the same qualitative behaviour. From a practical point of view we have achieved our control objective to keep the system (2.1) in a small neighbourhood of the origin. Therefore, if there exists an accessible component in a liquid rocket motor that can produce a naturally occurring feedback function $g(x) = [0, \alpha + \beta x_1 x_2]^T$, then we can achieve vibrational control by vibrating this component.

It is interesting and instructive to compare results obtained by this analysis with a numerical simulation. We can analytically solve the time averaged equation (3.12) to derive the following analytic expression for $Y_1(t)$

$$Y_1(t) = e^{-0.053t}[Y_1(0)\cos(1.03t) + Y_2(0)\sin(1.03t)], \tag{3.13}$$

where $Y_1(0)$ is the initial displacement and $Y_2(0)$ is the initial velocity. Figure (1) compares $Y_1(t)$ of (3.13) with a $X_1(t)$ calculated by numerically solving (3.7). Since the initial conditions for the slow solution $Y(t)$ are not known, they are matched to the initial conditions shown by the numerical simulation. Figure (1) shows that the slow equilibrium point $x = 0$ of the forced system (3.6) is indeed slowly asymptotically stable (i.e., $X_1(t)$ approaches a small asymptotically stable limit cycle) but is not asymptotically stable ($X_1(t) \not\to 0$). Furthermore, Fig. (1) shows excellent agreement between the behaviour predicted by the developed theory and the numerical simulation.

4 Conclusion

In this paper we present a criterion for nonlinear vibrational open loop control. Previous work that was restricted to linear control is extended to include analysis of nonlinear, vibrational control. It has been previously shown that linear vibrational control is not feasible if the Jacobian matrix has a positive trace. This paper demonstrates that nonlinear vibrational control is possible even if the trace of the Jacobian is positive. This result is significant because a large number of nonlinear engineering systems exhibit a positive Jacobian trace and yet may be stabilized by nonlinear, open loop, vibrational control. Finally, it is shown that the theory developed in this paper is in excellent agreement with numerical results.

5 Appendix

In this section we prove Theorem (2.1) and discuss the corresponding change of variables $x(t) = y(t) + u(t, y)$. We begin by assuming that the investigated system is described by

$$\dot{x} = f(x) + h(wt)g(x, w, a), \tag{5.1}$$

where $x(t) \in \mathbb{R}^n$, $f \in C^3(\mathbb{R}^n, \mathbb{R}^n)$, $f(0) = 0$, $h(wt) = \sin(wt)$, $w \gg 1$, and $g \in C^4(\mathbb{R}^n \times \mathbb{R} \times \mathbb{R}, \mathbb{R}^n)$. We perform a local analysis that will be restricted to a ball of radius δ centered at the origin. In addition, since w and a are constant, we write $g(x, w, a)$ simply as $g(x)$ and impose the following smoothness constraints

$$\begin{array}{lllll} \|f'(0)\| & \leq & \sigma, & 0 \leq & \sigma, \\ \|g(0)\| & \leq & w\delta_0, & 0 \leq & \delta_0, \\ \|g'(\xi)\| & \leq & w\delta_1, & 0 \leq & \delta_1, \end{array} \tag{5.2}$$

where $f'(x)$ denotes the derivative of f evaluated at x and $\xi \in B(0, \delta)$. To simplify the algebra, we introduce a fast time variable $s = wt$, define $\varepsilon = 1/w$, denote dx/ds as $\acute{x}$ and rewrite (5.1) in the fast time scale

$$\acute{x} = \varepsilon f(x) + \varepsilon h(s)g(x). \tag{5.3}$$

5.1 The Transformation

To prove Theorem (2.1) we introduce the change of variables $x(s) = y(s) + u(s,y)$. Next, we define the function $u(s,y)$ and determine some of its properties; that is,

$$u(s,y) = \alpha(y)\sin(s) + \beta(y)\cos(s), \tag{5.4}$$

where $\alpha(y), \beta(y) \in \mathbb{R}^n$. The functions $\alpha(y)$ and $\beta(y)$ are chosen so that $u(s,y)$ satisfies the partial differential equation

$$u_s(s,y) = \varepsilon J u(s,y) + \varepsilon h(s) g(y), \tag{5.5}$$

where $J = f'(0)$ is the Jacobian matrix and the subscript s denotes a partial derivative with respect to s. Note that for any fixed y the above equation is an ordinary differential equation in $u(\cdot, y)$. Substituting (5.4) into (5.5) and equating the coefficients of the sines and cosines yields

$$\begin{aligned} -\beta(y) - \varepsilon J\alpha(y) &= \varepsilon g(y), & (5.6)\\ \alpha(y) - \varepsilon J\beta(y) &= 0. & (5.7) \end{aligned}$$

Solving (5.6) and (5.7) for $\alpha(y)$ and $\beta(y)$ yields

$$\begin{aligned} \alpha(y) &= -\varepsilon^2[I + \varepsilon^2 J^2]^{-1} J g(y), & (5.8)\\ \beta(y) &= -\varepsilon J\alpha(y) - \varepsilon g(y), & (5.9) \end{aligned}$$

where the inverse matrix $[I+\varepsilon^2 J^2]^{-1}$ is well defined provided ε is small enough to satisfy the inequality $\|\varepsilon^2 J^2\| < 1$.

To derive approximate equations for $\alpha(y)$ and $\beta(y)$ we need the following bound on $g(y)$,

$$\|g(y)\| \le \|g(0) + g(y) - g(0)\| \le \|g(0)\| + \frac{\delta_1}{\varepsilon}\|y\| \le \frac{\delta_0 + \delta_1\delta}{\varepsilon}, \tag{5.10}$$

which holds for all $y \in B(0,\delta)$. Next, we represent the inverse matrix $[I + \varepsilon^2 J^2]^{-1}$ as the geometric series

$$[I + \varepsilon^2 J^2]^{-1} = I - \varepsilon^2 J^2 + \varepsilon^4 J^4 - \ldots = I + O(\varepsilon^2\sigma^2). \tag{5.11}$$

Using (5.8) through (5.11) yields the following approximate expressions

$$\begin{aligned} \alpha(y) &= -\varepsilon^2 J g(y) + O(\varepsilon^3\delta_0 + \varepsilon^3\delta\delta_1), & (5.12)\\ \beta(y) &= -\varepsilon g(y) + \varepsilon^3 J^2 g(y) + O(\varepsilon^4\delta_0 + \varepsilon^4\delta\delta_1). & (5.13) \end{aligned}$$

To complete the discussion of the properties of $u(s,y)$, we need bounds on $u(s,y)$ and the partial derivative $u_y(s,y)$. We begin by bounding the inverse matrix $[I + \varepsilon^2 J^2]^{-1}$. Equation (5.11) implies

$$\|[I + \varepsilon^2 J^2]^{-1}\| \le \|I\| + \varepsilon^2\|J^2\| + \ldots \le 1 + \varepsilon^2\sigma^2 + \ldots \le 1/(1 - \varepsilon^2\sigma^2). \tag{5.14}$$

It follows from (5.8), (5.9), (5.10) and (5.14) that

$$\begin{aligned} \|\alpha(y)\| &\le \frac{\varepsilon\sigma(\delta_0 + \delta\delta_1)}{1 - \varepsilon^2\sigma^2}, & (5.15)\\ \|\beta(y)\| &\le \frac{\delta_0 + \delta\delta_1}{1 - \varepsilon^2\sigma^2} & (5.16) \end{aligned}$$

for all $y \in B(0,\delta)$. To derive the desired bound on $u(s,y)$ we need only to note that (5.4) implies $\|u\| \le \|\alpha\| + \|\beta\|$, indicating that

$$\|u(s,y)\| \le \frac{(1+\varepsilon\sigma)(\delta_0 + \delta\delta_1)}{1 - \varepsilon^2\sigma^2} < 2(\delta_0 + \delta\delta_1) = O(\delta_0 + \delta\delta_1), \tag{5.17}$$

which holds for all s and sufficiently small ε. The bound on $u_y(s,y) = \alpha'(y)\sin(s) + \beta'(y)\cos(s)$ is also straightforward. Since (5.8) and (5.9) imply

$$\alpha'(y) = -\varepsilon^2[I + \varepsilon^2 J^2]^{-1} J g'(y), \tag{5.18}$$

$$\beta'(y) = -\varepsilon J \alpha'(y) - \varepsilon g'(y), \tag{5.19}$$

then using, (5.10), (5.14), (5.18) and (5.19) one obtains

$$\|u_y(s,y)\| \leq \frac{(1+\varepsilon\sigma)\delta_1}{1-\varepsilon^2\sigma^2} = O(\delta_1), \tag{5.20}$$

which holds for all s.

5.2 Proof of Theorem 2.1.

We begin by noting that the transformation $u(s,y)$ constructed in the previous section satisfies the constraints outlined in the theorem. The transformation $x(s) = y(s) + u(s,y)$ implies $dx/ds = \dot{x} = \dot{y} + u_s + u_y\dot{y}$. Substituting this relationship into (5.3) yields

$$[I + u_y(s,y)]\dot{y} + u_s(s,y) = \varepsilon f(y+u) + \varepsilon h(s) g(y+u). \tag{5.21}$$

Equation (5.20) implies $\|u_y(s,y)\| < 1$ for sufficiently small δ_1, for all $y \in B(0,\delta)$ and for all s. Consequently, the inverse matrix $[I + u_y(s,y)]^{-1}$ is well defined and we can rewrite (5.21) as

$$\dot{y} = [I + u_y(s,y)]^{-1}[\varepsilon f(y+u) + \varepsilon h(s) g(y+u) - u_s(s,y)]. \tag{5.22}$$

The following relationships will be used to simplify (5.22),

$$p(x) = f(x) - Jx, \tag{5.23}$$

$$q(y,u) = g(y+u) - g(y) - g'(y)u. \tag{5.24}$$

where $p(x)$ is defined as before and $q(y,u)$ represents the sum of all terms of second order and higher in the Taylor expansion of $g(y+u)$ around $u = 0$. It follows that

$$p(0) = 0, \quad p'(0) = 0, \quad p(x) = O(\|x\|^2), \tag{5.25}$$

$$q(y,0) = 0, \quad q_u(y,0) = 0, \quad q(y,u) = O(\|u\|^2). \tag{5.26}$$

Using (5.23) and (5.24) we can rewrite (5.22) as

$$\dot{y} = [I + u_y(s,y)]^{-1}[\varepsilon J y + \varepsilon J u(s,y) + \varepsilon p(y+u) + \varepsilon h(s) g(y) + \varepsilon h(s) g'(y) u(s,y) + \varepsilon h(s) q(y,u) - u_s(s,y)]. \tag{5.27}$$

Substituting (5.5) into (5.27) yields

$$\dot{y} = [I + u_y(s,y)]^{-1}[\varepsilon J y + \varepsilon p(y+u) + \varepsilon h(s) g'(y) u(s,y) + \varepsilon h(s) q(y,u)]. \tag{5.28}$$

Approximating the inverse matrix $[I + u_y(s,y)]^{-1}$ as a two term series with a second order error,

$$[I + u_y(s,y)]^{-1} = I - u_y(s,y) + O(\|u_y\|^2) = I - u_y(s,y) + O(\delta_1^2), \tag{5.29}$$

and substituting (5.29) into (5.28) yields

$$\dot{y} = \varepsilon[I - u_y(s,y) + O(\delta_1^2)][Jy + h(s) g'(y) u(s,y) + p(y + u(s,y)) + h(s) q(y, u(s,y))] = \varepsilon F(s,y). \tag{5.30}$$

We are now in a position to apply the method of averaging. Since $F(s,y)$ is periodic in s with a period 2π, we can approximate the non-autonomous system $\dot{y} = \varepsilon F(s,y)$ as the autonomous averaged system $\dot{y} = \varepsilon F_{av}(y)$ where

$$F_{av}(y) = \frac{1}{2\pi}\int_0^{2\pi} F(\tau, y) d\tau, \tag{5.31}$$

(see [9, p.412] for a discussion of averaging). Consequently, the averaged equation is given by

$$\dot{y} = \frac{\varepsilon}{2\pi}\int_0^{2\pi}[I - u_y(\tau,y) + O(\delta_1^2)][Jy + h(\tau)g'(y)u(\tau,y) + p(y+u(\tau,y)) + h(\tau)q(y,u(\tau,y))]d\tau. \tag{5.32}$$

Expanding (5.32) yields

$$\begin{aligned}\dot{y} \;= \tfrac{\varepsilon}{2\pi}\textstyle\int_0^{2\pi}[\;& Jy + h(\tau)g'(y)u(\tau,y) + p(y+u(\tau,y)) + h(\tau)q(y,u(\tau,y)) - u_y(\tau,y)Jy \\ & - u_y(\tau,y)h(\tau)g'(y)u(\tau,y) - u_y(\tau,y)p(y+u(\tau,y)) - u_y(\tau,y)h(\tau)q(y,u(\tau,y)) \\ & + O(\delta\delta_1^2 + \delta_0\delta_1^3/\varepsilon + \delta\delta_1^4/\varepsilon + \delta_0^2\delta_1^2)\;]d\tau.\end{aligned} \tag{5.33}$$

The terms $u_y(\tau,y)Jy$ and $u_y(\tau,y)h(\tau)g'(y)u(\tau,y)$ consist of an odd number of sinusoidal functions and thus average to zero. The term Jy is constant with respect to τ and can be taken outside the integral. Finally, since $h(s) = \sin(s)$ and $u(s,y) = \alpha(y)\sin(s) + \beta(y)\cos(s)$, then averaging the term $h(\tau)g'(y)u(\tau,y)$ yields

$$\frac{1}{2\pi}\int_0^{2\pi} h(\tau)g'(y)u(\tau,y)d\tau = \frac{1}{2\pi}\int_0^{2\pi} \sin^2(\tau)g'(y)\alpha(y) + \sin(\tau)\cos(\tau)g'(y)\beta(y)d\tau = g'(y)\alpha(y)/2. \tag{5.34}$$

Using the approximate expression (5.12) for $\alpha(y)$ in (5.34) lets us rewrite (5.33) as

$$\dot{y} = \varepsilon Jy - \frac{\varepsilon^3}{2}g'(y)Jg(y) + \frac{\varepsilon}{2\pi}\int_0^{2\pi}[p(y+u(\tau,y)) + h(\tau)q(y,u(\tau,y)) - u_y(\tau,y)p(y+u(\tau,y)) - u_y(\tau,y)h(\tau)q(y,u(\tau,y))]d\tau$$

$$+\varepsilon O(\varepsilon^2\delta_0\delta_1 + \delta\delta_1^2 + \delta_0\delta_1^3/\varepsilon + \delta\delta_1^4/\varepsilon + \delta_0^2\delta_1^2). \tag{5.35}$$

To complete the proof we have to bound the integral in the (5.35). The bounds on $u_y(\tau,y)p(y+u(\tau,y))$ and $u_y(\tau,y)h(\tau)q(y,u(\tau,y))$ follow from (5.17), (5.20), (5.25) and (5.26); that is,

$$u_y(\tau,y)p(y+u(\tau,y)) \;= O(\|u_y\|\|y+u\|^2) \;= O(\delta^2\delta_1 + \delta\delta_0\delta_1 + \delta_0^2\delta_1), \tag{5.36}$$

$$u_y(\tau,y)h(\tau)q(y,u(\tau,y)) \;= O(\|u_y\|\|u\|^2) \;= O(\delta_0^2\delta_1 + \delta\delta_0\delta_1 + \delta^2\delta_1^3). \tag{5.37}$$

In order to get bounds on the remaining terms, $p(y+u(\tau,y))$ and $h(\tau)q(y,u(\tau,y))$, we will require the following notation. Denote the second order Taylor expansion of $g(y+u)$ at $u=0$ as

$$g(y+u) = g(y) + g'(y)u + \frac{1}{2}g''(y)\langle u,u\rangle + O(\|u\|^3), \tag{5.38}$$

where $\langle u,u\rangle$ denotes a tensor and $g''(y)$ is the corresponding three dimensional array of coefficients evaluated at y. It follows that $q(y,u) = g''(y)\langle u,u\rangle/2 + O(\|u\|^3)$. Consequently, the average of $h(\tau)q(y,u(\tau,y))$ is written as

$$\frac{1}{2\pi}\int_0^{2\pi} h(\tau)q(y,u(\tau,y))d\tau = \frac{1}{4\pi}\int_0^{2\pi} h(\tau)g''(y)\langle u(\tau,y),u(\tau,y)\rangle d\tau + O(\|u\|^3). \tag{5.39}$$

Since each term of $h(\tau)\langle u(\tau,y),u(\tau,y)\rangle$ consists of an odd number of sinusoidal functions, the resulting average is zero. Hence, (5.39) is reduced to

$$\frac{1}{2\pi}\int_0^{2\pi} h(\tau)q(y,u(\tau,y))d\tau = O(\delta_0^3 + \delta\delta_0^2\delta_1 + \delta^2\delta_0\delta_1^2 + \delta^3\delta_1^3). \tag{5.40}$$

With the aid of the bounds (5.36), (5.37) and (5.40) we can rewrite (5.35) as

$$\dot{y} = \varepsilon Jy - \frac{\varepsilon^3}{2}g'(y)Jg(y) + \frac{\varepsilon}{2\pi}\int_0^{2\pi} p(y+u(\tau,y))d\tau + \varepsilon O(\varepsilon^2\delta_0\delta_1 + \delta\delta_1^2 + \delta_0\delta_1^3/\varepsilon + \delta\delta_1^4/\varepsilon + \delta_0^3 + \delta\delta_0\delta_1 + \delta_0^2\delta_1). \tag{5.41}$$

Equation (5.41) is of the form $\dot{y} = F(y) + \varepsilon O(\ldots)$ where

$$F(y) = \varepsilon J y - \frac{\varepsilon^3}{2} g'(y) J g(y) + \frac{\varepsilon}{2\pi} \int_0^{2\pi} p(y + u(\tau, y)) d\tau. \tag{5.42}$$

Since we are concerned with local behaviour at the origin, we linearize (5.41) about $y = 0$, to get

$$\dot{y} = F(0) + \left[\frac{\partial F}{\partial y}(0) \right] y + \varepsilon O(\delta^2 + \ldots). \tag{5.43}$$

Expanding the above yields

$$\dot{y} = \left[\frac{\varepsilon}{2\pi} \int_0^{2\pi} p(u(\tau, 0)) d\tau - \frac{\varepsilon^3 g'(0) J g(0)}{2} \right] + \varepsilon J y - \frac{\varepsilon^3}{2} \left[\frac{\partial (g'(y) J g(y))}{\partial y}(0) \right] y + \left[\frac{\partial \left(\frac{\varepsilon}{2\pi} \int_0^{2\pi} p(y + u(\tau, y)) d\tau \right)}{\partial y}(0) \right] y$$

$$+ \varepsilon O(\delta^2 + \varepsilon^2 \delta_0 \delta_1 + \delta \delta_1^2 + \delta_0 \delta_1^3 / \varepsilon + \delta \delta_1^4 / \varepsilon + \delta_0^3 + \delta \delta_0 \delta_1 + \delta_0^2 \delta_1). \tag{5.44}$$

We now complete the proof by bounding the last term in (5.44). Since the derivative of $p(x)$ exists and is continuous by assumption, we can move the partial derivative $\partial / \partial y$ inside the integral to get

$$\left[\frac{\partial \left(\frac{\varepsilon}{2\pi} \int_0^{2\pi} p(y + u(\tau, y)) d\tau \right)}{\partial y}(0) \right] = \frac{\varepsilon}{2\pi} \int_0^{2\pi} \left\{ \frac{\partial [p(y + u(\tau, y))]}{\partial y}(0) \right\} d\tau \tag{5.45}$$

where

$$\frac{\partial [p(y + u(\tau, y))]}{\partial y}(0) = p'(u(\tau, 0)) + p'(u(\tau, 0)) u_y(\tau, 0). \tag{5.46}$$

Since $p(x) \in \mathbb{R}^n$, then $p'(a) \in \mathbb{R}^{n \times n}$ is a matrix valued function. Letting $[M]_{ij}$ denote the ij'th element of the matrix M and $\ell_{ij}(a) = [p'(a)]_{ij} \in \mathbb{R}$, then using (5.46) lets us write the ij'th term of (5.45) as

$$\left[\frac{\partial \left(\frac{\varepsilon}{2\pi} \int_0^{2\pi} p(y + u(\tau, y)) d\tau \right)}{\partial y}(0) \right]_{ij} = \frac{\varepsilon}{2\pi} \int_0^{2\pi} \ell_{ij}(u(\tau, 0)) + \langle \ell_{ik}(u(\tau, 0)) [u_y(\tau, 0)]_{kj} \rangle d\tau, \tag{5.47}$$

where the tensor notation $\langle\ \rangle$ implies a summation over the index k. Expanding ℓ_{ij} and ℓ_{ik} as first and zero order Taylor series about the origin yields

$$\left[\frac{\partial \left(\frac{\varepsilon}{2\pi} \int_0^{2\pi} p(y + u(\tau, y)) d\tau \right)}{\partial y}(0) \right]_{ij} = \frac{\varepsilon}{2\pi} \int_0^{2\pi} \left\{ \ell_{ij}(0) + \ell'_{ij}(0) u(\tau, 0) + \langle \ell_{ik}(0) [u_y(\tau, 0)]_{kj} \rangle \right\} d\tau + \varepsilon O(\|u\|^2 + \|u\| \|u_y\|). \tag{5.48}$$

Equation (5.25) implies $\ell_{ij}(0) = 0$ and the averages of $\ell'_{ij}(0) u(\tau, 0)$ and $\ell_{ik}(0) [u_y(\tau, 0)]_{kj}$ are zero. Consequently,

$$\left[\frac{\partial \left(\frac{\varepsilon}{2\pi} \int_0^{2\pi} p(y + u(\tau, y)) d\tau \right)}{\partial y}(0) \right] y = \varepsilon O(\|y\| \|u\|^2 + \|y\| \|u\| \|u_y\|) = O(\delta \delta_0^2 + \delta \delta_0 \delta_1 + \delta^2 \delta_1^2). \tag{5.49}$$

The bound (5.49) allows us to rewrite (5.44) as

$$\dot{y} = \left[\frac{\varepsilon}{2\pi} \int_0^{2\pi} p(u(\tau, 0)) d\tau - \frac{\varepsilon^3 g'(0) J g(0)}{2} \right] + \varepsilon J y - \frac{\varepsilon^3}{2} \left[\frac{\partial (g'(y) J g(y))}{\partial y}(0) \right] y +$$

$$\varepsilon O(\delta^2 + \varepsilon^2 \delta_0 \delta_1 + \delta \delta_1^2 + \delta_0 \delta_1^3 / \varepsilon + \delta \delta_1^4 / \varepsilon + \delta_0^3 + \delta_0^2 \delta_1 + \delta \delta_0^2 + \delta \delta_0 \delta_1). \tag{5.50}$$

According to the definition (2.4)

$$\phi(\tau) = -\varepsilon^2 Jg(0)\sin(\tau) - \varepsilon g(0)\cos(\tau), \tag{5.51}$$

then (5.12) and (5.13) imply

$$\phi(\tau) = u(\tau, 0) + O(\varepsilon^3\delta_0 + \varepsilon^3\delta\delta_1). \tag{5.52}$$

Using (5.52) in (5.50) yields

$$\dot{y} = \left[\frac{\varepsilon}{2\pi}\int_0^{2\pi} p(\phi(\tau))d\tau - \frac{\varepsilon^3 g'(0)Jg(0)}{2}\right] + \varepsilon Jy - \frac{\varepsilon^3}{2}\left[\frac{\partial(g'(y)Jg(y))}{\partial y}(0)\right] y +$$

$$\varepsilon O(\delta^2 + \varepsilon^2\delta_0\delta_1 + \delta\delta_1^2 + \delta_0\delta_1^3/\varepsilon + \delta\delta_1^4/\varepsilon + \delta_0^3 + \delta_0^2\delta_1 + \delta\delta_0^2 + \delta\delta_0\delta_1 + \varepsilon^3\delta_0^2). \tag{5.53}$$

Rewriting (5.53) in the original time scale t yields

$$\dot{y} = Ay + b + O(\zeta). \tag{5.54}$$

where A, b and ζ are as defined in the theorem. □

5.3 Choice of $g(x)$ in Positive Trace Example

In equation (3.5) we let $g(x) = [0, \alpha + \beta x_1 x_2]^T$. This hypothetical choice of $g(x)$ is not arbitrary. We know that the sign of A_1 creates an instability. Consequently we wish to change the sign of this coefficient by applying vibrational control. Consider the averaged equation (2.8). If we denote the vector $g'(x)Jg(x)$ as $[G_1(x), G_2(x)]^T$ then the matrix A defined in (2.6) can be written as

$$A = J - k\frac{\partial[G_1(x), G_2(x)]^T}{\partial x}(0) = J - k\begin{bmatrix} \partial G_1(0)/\partial x_1 & \partial G_1(0)/\partial x_2 \\ \partial G_2(0)/\partial x_1 & \partial G_2(0)/\partial x_2 \end{bmatrix} \tag{5.55}$$

where k is a positive constant. For A to have a negative trace either $\partial G_1(0)/\partial x_1$ or $\partial G_2(0)/\partial x_2$ must be positive, or both. Consequently, letting $\partial G_2(0)/\partial x_2 = c$ be a positive quantity implies $G_2(x) = cx_2$. It follows that

$$G_2(x) = g_2(x)\frac{\partial g_2}{\partial x_1} - g_1(x)\frac{\partial g_2}{\partial x_2} + 0.2g_2(x)\frac{\partial g_2}{\partial x_2} = cx_2. \tag{5.56}$$

If we consider the first term only, we can set

$$g_2(x)\frac{\partial g_2}{\partial x_1} = cx_2. \tag{5.57}$$

Equation (5.57) is a partial differential equation in $g_2(x)$, which can be solved by separation of variables. Unfortunately, the solution to (5.57) is $g_2(x) = \pm c_1\sqrt{|x_1 x_2|}$ which is singular at the origin and violates the assumption that $g(x)$ is continuously differentiable. Consequently, we let $g_2(x) = \alpha + \beta x_1 x_2$, approximating the square root dependance of $g_2(x)$ near the origin. If we now set $g_1(x) = 0$, then $g(x) = [0, \alpha + \beta x_1 x_2]^T$. It is noteworthy that the last term in (5.56) suggests that $g_2(x) = Kx_2$ might also be a viable feedback function. Such a choice requires, however, that $K > w$, which violates the assumption that $\|g'(x)\| \leq w\delta_1 < w$.

References

[1] R.E. Bellman, J. Bentsman, and S.M Meerkov. "Vibrational control of nonlinear systems: vibrational stabilizability". *IEEE Transactions on Automatic Control*, vol.AC-31:pp.710–724, Aug 1986.

[2] S.M. Meerkov and G.I. Shapiro. "Method of vibrational control in the problem of stabilization of ionization-thermal instability of a powerful continuous CO_2 laser". *Automatic Remote Control*, vol.37:pp.821–830, 1976.

[3] C. McGreavy and J.M. Thornton. "Stability studies of single catalyst particles". *Chemical Engineering*, vol.1:pp.296–301, 1970.

[4] S.M. Meerkov. "Principle of vibrational control: theory and applications". *IEEE Transactions on Automatic Control*, vol.AC-25:pp.755–762, Aug 1980.

[5] J. Guckenheimer and P. Holmes. *Nonlinear oscillations, dynamical systems, and bifurcations of vector fields.* New York: Springer Verlag, 1983.

[6] J. Bentsman. "Vibrational control of a class of nonlinear systems by nonlinear multiplicative vibrations". *IEEE Transactions on Automatic Control*, vol.AC-32:pp.711–716, Aug 1987.

[7] G. Strang. *Linear Algebra and its Applications.* New York: Harcourt Brace Jovanovich, Inc., 1988.

[8] E. Powell. *Nonlinear combustion instability in liquid propellant rocket engines.* PhD thesis, Georgia Institute of Technology, 1970.

[9] H.K. Khalil. *Nonlinear Systems.* New York: Macmillan Publishing Company, 1992.

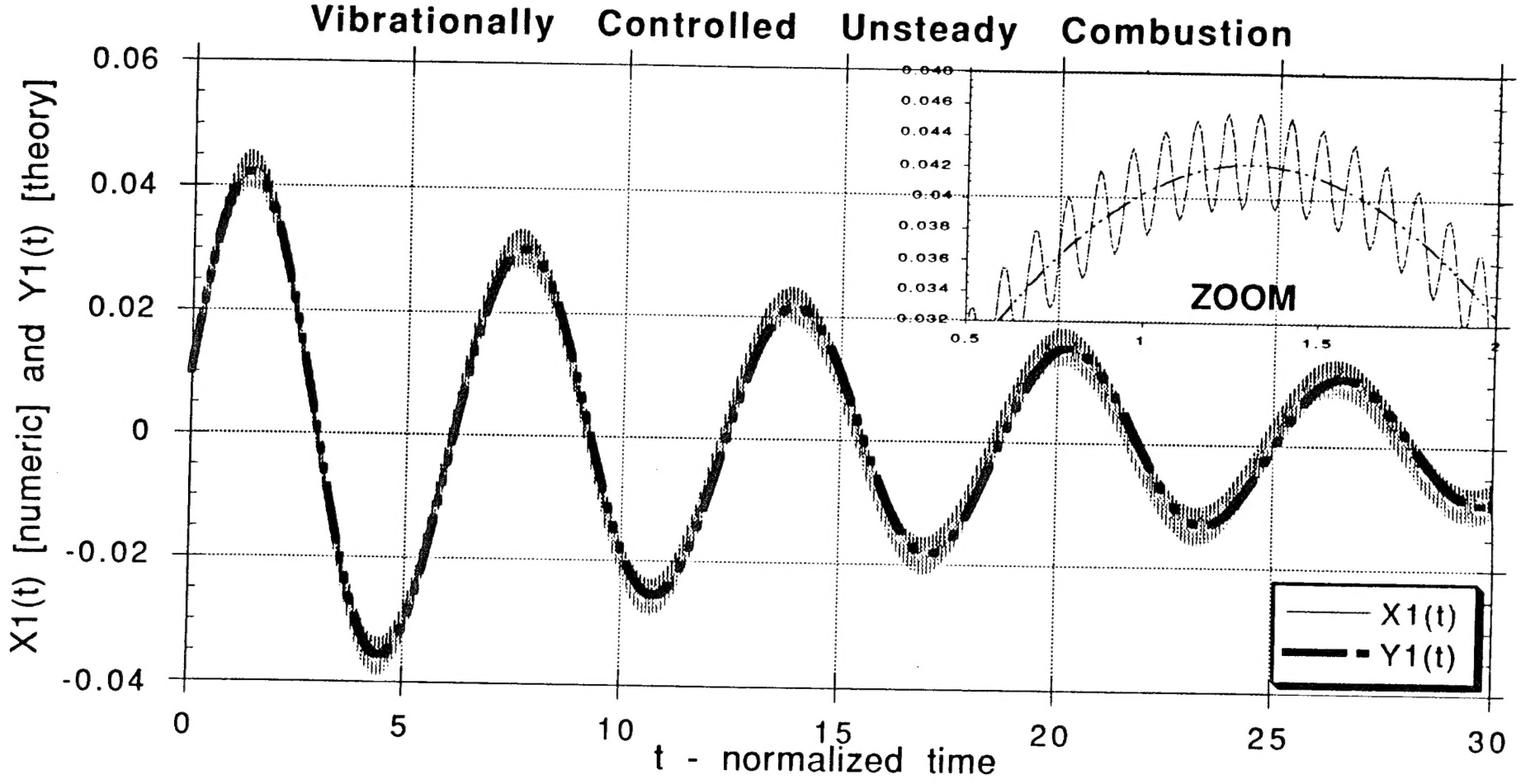

Figure 1: Damping of a liquid rocket instability by high frequency vibrational control